博士論文

A novel IRE1 signaling triggered by membrane lipid saturation

(小胞体ストレス応答分子 IRE1 を介した

膜脂肪酸ストレス応答機構の解明)

大場 陽介

Table of contents

Abbreviations

AMPK: 5' adenosine monophosphate (AMP)-activated protein kinase

ATF6: activating transcription factor 6

Bip: binding immunoglobulin protein

CHOP: C/EBP homology protein

DNAJB9: DnaJ homolog, subfamily B, member 9

IRE1: inositol-requiring enzyme 1

MUFA: monounsaturated fatty acid

PERK: protein kinase RNA (PKR)-like ER kinase

PRKAG2: Protein kinase AMP activated gamma 2

SCD: stearoyl-CoA desaturase

SFA: saturated fatty acid

UPR: unfolded protein response

Tm: tunicamycin

XBP1: X-box binding protein 1

Introduction

Phospholipids are major and key components of cellular membranes of all living cells. Fatty acids in membrane phospholipids of mammalian cells exhibit considerable structural diversity, including varying chain lengths and degrees of unsaturation (Lands and Crawford, 1976; Holub and Kuksis, 1978; MacDonald and Sprecher, 1991). It has been shown that the fatty acyl moieties of the phospholipid bilayer influence the biophysical properties of cellular membranes, such as the degree of membrane fluidity and the function or localization of membrane-associated proteins (Spector and Yorek, 1985).

The fatty acid composition of phospholipid is likely to be affected by the exogenous fatty acid from the diet or by altered activities of lipid-metabolizing enzymes. So far, several cellular responses to changes in phospholipid fatty acid composition have been found in micro-organisms. In the cyanobacterium, the palladium-catalyzed hydrogenation of membrane lipids stimulated the expression of the desA gene, which is responsible for the desaturation of fatty acids of membrane lipids (Vigh *et al*., 1993). Gene-engineered rigidity of the membrane was also reported to enhance the inducible expression of cold-inducible genes (Inaba *et al*., 2003). However, homeostatic responses to changes in membrane fatty acid composition have been poorly understood in mammalian cells.

Our laboratory previously found that palmitic acid treatment or knockdown of stearoyl-CoA desaturase 1 (SCD1) promotes an increase of saturated fatty acids (SFAs) in membrane phospholipids (hereafter referred to as ‘membrane lipid saturation’) and

activates the unfolded protein response (UPR) in HeLa cells (Ariyama *et al*., 2010). The UPR is a transcriptional and translational intracellular signaling pathway activated by the accumulation of unfolded proteins in the lumen of the endoplasmic reticulum (ER). The UPR is mediated by at least three transmembrane proteins, including inositol-requiring enzyme 1 (IRE1), PKR-like ER kinase (PERK), and activating transcription factor 6 (ATF6) (Figure 1). Under unstressed condition, these proteins are maintained in an inactive state by binding to the major ER chaperone, immunoglobulin heavy chain binding protein/glucose regulated protein 78 (Bip/GRP78), at the side of the ER lumen. During unfolded protein accumulation in the ER (ER stress), Bip is displaced to interact with unfolded luminal proteins, resulting in the release of IRE1, PERK and ATF6, and leading to their activation (Walter and Ron, 2011). Signaling by these sensors up-regulates transcription of UPR target genes, including ER chaperones and ER-associated degradation (ERAD) components. The UPR also attenuates cellular protein synthesis, thereby reducing the unfolded protein load (Ron and Walter, 2007).

In addition to its role in protein quality control in the ER, the UPR is known to control membrane lipid biosynthesis. XBP1 activates the phosphatidylcholine biosynthesis pathway at least by increasing the level of choline cytidylyltransferase protein, a rate-limiting enzyme in the cytidine diphosphocholine (CDP-choline) pathway (Sriburi *et al*., 2004; Sriburi *et al.*, 2007). ATF6 also induces phosphatidylcholine biosynthesis by increasing the activity of choline kinase, the first enzyme in the CDP-choline pathway (Bommiasamy *et al*., 2009). Given that protein secretion requires ER expansion and the trafficking of secretory vesicles, it makes sense

that the UPR also activates lipid synthesis to meet the demand of lipid bilayer formation. On the other hand, the fact that the UPR regulates membrane lipid metabolism raises the possibility that the UPR acts as a homeostatic response of membrane lipids. However, it is unclear whether the UPR is adaptive response to membrane lipid saturation, and if so, how cells adapt to membrane lipid saturation through activating the UPR.

In this study, I identified a novel IRE1 signaling triggered by membrane lipid saturation. In the downstream of IRE1 activation, I found that membrane lipid saturation activated AMP-dependent protein kinase (AMPK) via IRE1 activation. The AMPK activation was dependent on AMPKγ2, one of AMPK subunits, that was up-regulated by IRE1 upon membrane lipid saturation. Activated AMPK induced SCD1 expression to reduce accumulation of SFA, which causes membrane lipid saturation and cytotoxicity. Interestingly, these IRE1-dependent phenomena were completely independent of XBP1, a major downstream effector of IRE1, and not triggered by unfolded protein accumulation. Taken together, these findings reveal that IRE-AMPK axis plays an important role in membrane fatty acid homeostasis.

Results

IRE1 knockdown enhances apoptosis triggered by membrane lipid saturation

A previous study has shown that IRE1 and PERK are selectively activated by membrane lipid saturation (Kitai *et al*., 2013). To determine whether IRE1 and/or PERK are required for adaptation to membrane lipid saturation, I knockdown IRE1 or PERK in HeLa cells and then treated these cells with palmitic acid (16:0), a representative SFA. Consistent with previous studies (Cazanave *et al.*, 2009), treatment with 100 μM palmitic acid for 12 h caused cell death. IRE1 knockdown didn't affect cell survival under the normal culture conditions, but markedly enhanced the palmitic acid-induced cell death. On the other hand, PERK knockdown didn't affect the survival of cells regardless of palmitic acid treatment (Figure 2A).

When IRE1 is activated under ER stress condition, it splices the XBP1 mRNA. The spliced XBP1 (XBP1s) mRNA is translated into a functional transcription factor to up-regulate gene expression for ER quality control (Cox and Walter, 1996; Calfon *et al*., 2002). Since XBP1 splicing also occurs when cells are treated with palmitic acid (Ariyama *et al*., 2010), I examined the effect of XBP1 knockdown on the palmitic acid-induced toxicity. To my surprise, I found that XBP1 knockdown didn't enhance palmitic acid-induced cell death (Figure 2A). I also performed immunoblot analysis of cleaved caspase3, one of important apoptosis-associated factors. As shown in Figure 2B, palmitic acid-induced caspase3 cleavage was enhanced by IRE1 knockdown, but not by XBP1 knockdown.

Stearoyl-CoA desaturase 1 (SCD1) catalyzes the conversion from the SFAs, palmitic acid (16:0) and stearic acid (18:0) to the monounsaturated fatty acids (MUFAs), palmitoleic acid (16:1) and oleic acid (18:1), respectively. Since inhibition of SCD1 is known to induce membrane lipid saturation (Ariyama *et al*., 2010), I used SCD1 inhibitor (CAY10566) (Liu *et al*., 2007) as another membrane lipid saturation inducer. The cell death and caspase3 cleavage induced by SCD1 inhibitor were also enhanced by IRE1 knockdown (Figure 3). In contrast, XBP1 knockdown didn't enhance the SCD1 inhibitor-induced apoptosis (Figure 3). These results suggest that IRE1 suppress apoptosis induced by membrane lipid saturation in an XBP1-independent manner.

AMPKγ2 (PRKAG2) expression is increased by membrane lipid saturation

The above results led me to hypothesis that an yet identified IRE1 signaling pathway is activated by membrane lipid saturation. To explore the signaling pathway, I first carried out gene expression analysis. I performed DNA microarray analysis in HeLa cells treated with control or IRE1 siRNA and examined gene expression profiles under vehicle, palmitic acid or SCD1 inhibitor treatment (Figure 4). First, I picked up genes as membrane lipid saturation-responsive and IRE1-dependent genes based on 2 criteria: (1) in control siRNA-treated cells, they were up-regulated more than 2-fold by both palmitic acid and SCD1 inhibitor treatment, and (2) in IRE1 siRNA-treated cells, they were up-regulated less than 2-fold by both palmitic acid and SCD1 inhibitor treatment. Then I confirmed the reproducibility of the microarray results and examined the XBP1 dependency, the criteria of which are same as IRE1 dependency, by

quantitative realtime PCR (qRT-PCR). As a result, I identified 10 genes which were elevated more than 2-fold by membrane lipid saturation in an IRE1-dependent manner (Figure 5). Among them, Protein kinase AMP-activated gamma 2 (PRKAG2) mRNA was up-regulated about 4-fold by both palmitic acid and SCD1 inhibitor treatment, and the up-regulations were significantly suppressed by IRE1 knockdown, but not by XBP1 knockdown (Figure 6). PRKAG2 encodes AMP-activated protein kinase gamma subunit 2, so hereafter I refer to PRKAG2 as AMPKγ2. Next, to further confirm the XBP1 dependency, I generated a HeLa cell line stably expressing XBP1s by retrovirus infection. In the XBP1s-expressing cells, mRNA levels of XBP1s and one of its downstream genes, DnaJ homolog, subfamily B, member 9 (DNAJB9), were increased compared with control cells (Figure 7A). mRNAs of FBXO16 and PPAPDC1B, newly identified IRE1/XBP1-dependent genes (Figure 5) were also highly elevated in the cells, but AMPKγ2 mRNA was hardly elevated (Figure 7B). A conventional ER stressor, tunicamycin, which causes the accumulation of unfolded proteins in ER, didn't induce AMPKγ2 expression at all, although IRE1 was activated (Figure 8). These results indicate that AMPKγ2 is up-regulated by membrane lipid saturation via IRE1 but not XBP1.

Next, I knockdown AMPKγ2 and then treated with palmitic acid or SCD1 inhibitor. The efficiency of siRNA-mediated knockdown of AMPKγ2 was evaluated by qRT-PCR (Figure 9C). Similar to IRE1 knockdown, AMPKγ2 knockdown enhanced both palmitic acid- and SCD1 inhibitor-induced cell death (Figures 9A and 10A). AMPKγ2 knockdown also increased the level of cleaved caspase3 when treated with

palmitic acid and SCD1 inhibitor (Figures 9B and 10B). These results suggest that AMPKγ2, which is up-regulated by lipid membrane saturation in an IRE1-dependent/XBP1-independent manner, plays a role in suppressing membrane lipid saturation-induced apoptosis.

Membrane lipid saturation induces AMPK activation

The AMP-activated protein kinase (AMPK) is an evolutionarily conserved serine/threonine kinase that functions as a sensor of cellular energy and nutrient status (Mihaylova and Shaw, 2011). In general, AMPK monitors the ratio of AMP/ATP and, if an energy deficit (an increase in AMP/ATP ratio) is detected, acts to restore energy homeostasis by switching on catabolic pathways that produce ATP while switching off biosynthetic pathways and other nonessential processes consuming ATP. AMPK exists as an obligate heterotrimer, containing a catalytic subunit (α), and two regulatory subunits (β and γ). Each subunit has multiple isoforms (α1, α2, β1, β2, γ1, γ2, and γ3) and AMPKγ2 is one of the three γ subunit isoforms. Phosphorylation of Thr172 in the activation loop of AMPKα is required for AMPK activation, and is promoted by the binding of AMP to the AMPKγ subunit (Hardie *et al*., 2012).

A previous study has shown that AMPK activity is increased in cell lysates from cardiomyocytes adenovirally transduced with AMPKγ2 gene (Folmes *et al*., 2009). Consistently, expression of AMPKγ2 COOH-terminally tagged with FLAG or myc in HeLa cells increased Thr172 phosphorylation of AMPK α (Figure 11), indicating that AMPK was activated by increased expression of AMPKγ2. These results led me to

led me to investigate whether AMPK is activated by membrane lipid saturation. Strikingly, treatment with palmitic acid or SCD1 inhibitor time-dependently increased Thr172 phosphorylation of AMPKα (Figure 12). Moreover, IRE1 knockdown, but not XBP1 knockdown, largely suppressed the phosphorylation of AMPKα by palmitic acid or SCD1 inhibitor treatment (Figures13 and 14). AMPKγ2 knockdown also suppressed the AMPKα phosphorylation by palmitic acid or SCD1 inhibitor but didn't affect IRE1 activation (Figure 15). In contrast to palmitic acid or SCD1 inhibitor treatment, tunicamycin treatment didn't cause AMPKα phosphorylation at all (Figure 16). These results indicate that membrane lipid saturation but not unfolded protein accumulation causes AMPK activation, which is dependent on IRE1 and AMPKγ2, but not on XBP1.

To elucidate whether AMPK is involved in palmitic acid-induced apoptosis, I knockdown AMPKα, a catalytic subunit of AMPK, in HeLa cells and then treated with palmitic acid. The efficiency of siRNA-mediated knockdown of AMPKα was evaluated by immunoblot (Figure 17B). Similar to IRE1 and AMPKγ2 knockdown, AMPKα knockdown increased cell death and the level of cleaved caspase3 in palmitic acid-treated cells, although AMPKα knockdown itself didn't affect cell survival (Figure 17). These results suggest that IRE1- and AMPKγ2-mediated AMPK activation is important to suppress apoptosis triggered by membrane lipid saturation.

IRE1 and AMPK knockdown increases SFA accumulation in palmitic acid-treated cells

Since AMPK regulates several metabolic pathways, AMPK activation by membrane lipid saturation led me to focus on the intracellular fatty acid metabolism. I measured the intracellular fatty acid composition of HeLa cells treated with palmitic acid by GC-MS analysis. The cellular proportion of SFA to MUFA (SFA/MUFA ratio) was almost 1 in untreated cells but was increased to more than 2 by palmitic acid treatment (Figure 18). Treatment of AMPKα siRNA and Compound C, an inhibitor of AMPK (Zhou *et al*., 2001), both of which inhibit AMPK signaling, increased the cellular SFA/MUFA ratio in palmitic acid-treated cells (Figure 18). Similarly, AMPKγ2 knockdown augmented the SFA/MUFA ratio when treated with palmitic acid (Figure 19). Furthermore, IRE1 knockdown, but not XBP1 knockdown, enhanced the SFA/MUFA ratio in cells treated with palmitic acid (Figure 20). Taken together, these results suggest that IRE1-mediated AMPK activation is important to reduce SFA accumulation in palmitic acid-treated cells.

IRE1 and AMPK promote fatty acid desaturation in palmitic acid-treated cells

The elevated SFA/MUFA ratio in IRE1 or AMPK subunit knockdown cells treated with palmitic acid led me to hypothesis that fatty acid desaturation is affected in these cells. To investigate the desaturation of incorporated palmitic acid, I used [^{14}C]-labeled palmitic acid. In mammals, SFAs incorporated into cells are converted to MUFAs by introduction of a double bond. HeLa cells were cultured in the medium containing

[^{14}C]-labeled palmitic acid, and then radiolabeled fatty acids extracted from cells were analyzed by silver nitrate thin-layer chromatography ($AgNO_3$-TLC) (Wilson and Sargent, 2001). In control cells, about 15% of incorporated palmitic acid was converted to MUFAs, and the conversion was significantly reduced in IRE1 but not XBP1 knockdown cells (Figure 21). Similar to IRE1 knockdown, AMPKγ2 or AMPKα knockdown, or treatment with compound C, all of which inhibit AMPK signaling decreased the conversion of incorporated palmitic acid to MUFAs (Figure 22). These results indicate that increased SFA accumulation in IRE1 and AMPK knockdown cells is caused by the reduction of fatty acid desaturation.

SCD1 is up-regulated by membrane lipid saturation in an IRE1- and AMPK-dependent manner

Since SCD1 is one of the main enzymes of SFA desaturation in mammals, I next examined whether the expression of SCD1 is changed by membrane lipid saturation. Both of the mRNA and protein levels of SCD1 were induced by palmitic acid treatment, and the increased expression was inhibited by knockdown of IRE1 but not XBP1 (Figure 23). AMPKγ2 or AMPKα knockdown, or treatment of compound C also inhibited palmitic acid-mediated induction of SCD1 in both mRNA and protein levels (Figure 24). In SCD1 inhibitor-treated cells, the expression level of SCD1 was elevated as in palmitic acid-treated cells, and IRE1 but not XBP1 knockdown inhibited its increase (Figure 25). Furthermore, knockdown of AMPK subunits or compound C treatment also inhibited SCD1 protein increase triggered by SCD1 inhibitor treatment

(Figure 26). On the other hand, tunicamycin treatment didn't change either mRNA or protein expression levels of SCD1 although it activated IRE1 (Figure 27). These results suggest that membrane lipid saturation, but not unfolded protein accumulation, causes up-regulation of SCD1 in an IRE1- and AMPK- dependent manner, which in turn promotes SFA desaturation.

The stability of AMPKγ2 mRNA is elevated by membrane lipid saturation

IRE1 is an ER transmembrane protein that activates the UPR to maintain the ER homeostasis. IRE1 triggers the UPR through a cytoplasmic kinase domain and an RNase domain. Upon ER stress, RNase of IRE1 is activated through dimerization, trans-autophosphorylation, and higher-order conformational change, which leads to splicing of XBP1 mRNA (Cox and Walter, 1996; Calfon *et al*., 2002). I examined whether RNase activity of IRE1 is required for AMPKγ2 mRNA up-regulation in membrane lipid saturation. 4μ8C is a recently described IRE1 inhibitor that specifically inhibits the RNase activity of IRE1 and prevents splicing of the XBP1 mRNA in response to ER stress (Cross *et al*., 2012). 4μ8C partially inhibited the palmitic acid-induced splicing of XBP1 mRNA and expression of DNAJB9 mRNA, in a dose-dependent manner (Figures 28B and C). Similarly, 4μ8C partially inhibited the palmitic acid-induced expression of AMPKγ2 mRNA (Figure 28A). The result implies that RNase activity of IRE1 is involved in the elevation of AMPKγ2 mRNA by membrane lipid saturation.

In addition to site-specific RNase activity (leading to XBP1 mRNA splicing), mammalian IRE1 has also been implicated in the degradation of diverse mRNAs encoding secreted proteins, which process is referred to as regulated IRE1-dependent decay of mRNA (RIDD) (Maurel *et al*., 2014). Furthermore, recent studies reported that IRE1 degrades some micro RNAs (miRNAs) (Upton *et al*., 2012; Lerner *et al*., 2012). Since mRNA stability is often governed by binding of specific miRNAs to complementary sequences in the 3' untranslated region (UTR) of gene targets, I asked whether the induction of AMPKγ2 mRNA upon membrane lipid saturation is due in part to changes in its mRNA stability. I measured the stability of AMPKγ2 mRNA using actinomycin D (ActD), which blocks transcription. I found that AMPKγ2 mRNA was relatively labile but significantly stabilized when treated with palmitic acid (Figure 29A). On the other hand, tunicamycin didn't change its stability (Figure 29C) in agreement with the result that AMPKγ2 mRNA was not induced by tunicamycin treatment. Furthermore, palmitic acid-induced stabilization of AMPKγ2 mRNA was not observed in IRE1 knockdown cells (Figure 29B), indicating that IRE1 is required for stabilizing AMPKγ2 mRNA during palmitic acid treatment. These results suggest that AMPKγ2 up-regulation, at least in part, results from stabilization of its mRNA and raise the possibility that IRE1 degrades miRNAs that target the 3' UTR of AMPKγ2 mRNA.

Discussion

In this study, I revealed that AMPKγ2, one of AMPK subunits, is induced and AMPK is activated by the UPR sensor IRE1 in both palmitic acid- and SCD1 inhibitor-treated HeLa cells. I also found that SCD1 is up-regulated in these cells at the downstream of IRE1 and AMPK activation to promote SFA desaturation, which is required for membrane lipid homeostasis and cell survival (Figure 31).

Since exogenously supplied palmitic acids not only exist as non-esterified form in the cell but also are incorporated into neutral fatty acids or phospholipid, it is possible that each lipid fraction triggers the signaling. However, I showed that SCD1 inhibitor treatment, which causes the increase of SFA only in membrane phospholipids (i.e., membrane lipid saturation), also evokes the same signaling. From these results, I assume that the signaling discovered in this study is triggered by membrane lipid saturation.

I found that IRE1 and AMPK inhibition enhance apoptosis triggered by membrane lipid saturation. In IRE1- and AMPK- inhibited cells, the SFA/MUFA ratio is increased by the treatment of palmitic acid, suggesting that excess SFA accumulation in membrane lipid causes apoptosis. Although both IRE1 signaling and AMPK signaling have been reported to promote apoptosis (Urano *et al*., 2000; Nishitoh *et al.*, 2002; Okoshi *et al*., 2008), apoptosis induced by membrane lipid saturation was enhanced in the condition of IRE1 or AMPK inhibition, suggesting that another apoptotic stimulating signaling is activated in that condition. One possible candidate is PERK mediated signaling. In the case of prolonged or severe ER stress, PERK

generates pro-apoptotic signals by up-regulation of CHOP and other PERK-dependent proteins (McCullough *et al*., 2001; Marciniak *et al*., 2004). It has been reported that PERK is also activated by membrane lipid saturation, and PERK knockdown suppresses SCD1 knockdown mediated apoptosis (Ariyama *et al*., 2010; Kitai *et al.*, 2013). Another possibility is c-Src-mediated Jun N-terminal kinase (JNK) signaling. Palmitic acid induces c-Src clustering within membrane subdomains, which in turn activate JNK (Holzer *et al*., 2011). JNK is known to be involved in saturated fatty acid-induced apoptosis by activating the pro-apoptotic Bcl-2 proteins Bim and Bax (Malhi *et al.*, 2006). Further studies are needed to determine which signaling pathway mediates apoptosis triggered by membrane lipid saturation.

I demonstrated that the phosphorylation at Thr172 of AMPKα is activated by membrane lipid saturation in an IRE1- and AMPKγ2- dependent manner. I also found that membrane lipid saturation up-regulates AMPKγ2 via IRE1, and overexpression of AMPKγ2 induces Thr172 phosphorylation of AMPK α. In mammals, the major upstream kinases of AMPK are the LKB1-STRAD-MO25 complex and the Ca^{2+}/calmodulin-activated protein kinase kinases 2 (CaMKK2) (Woods *et al*., 2003; Hawley *et al.*, 2005). Additional studies have suggested the MAPKKK (mitogen-activated protein kinase kinase kinase) family member TGF-β activated kinase 1 (TAK1) phosphorylates Thr172 (Momcilovic *et al.*, 2006). Considering the fact that HeLa cells do not express LKB1, activated IRE1 may induce the activity of CaMKK2, TAK1 and/or unknown kinases by membrane lipid saturation.

AMPKγ2 is one of three γ subunits of AMPK, and the γ isoforms have the

greatest structural variability (Moffat and Harper, 2010). The γ1 subunit is the smallest at 331 residues and is expressed in almost every cell type and tissue. The γ3 subunit is larger at 489 residues and is the most restricted in its tissue expression, only in skeletal muscle. The γ2 subunit is by far the largest isoform at 569 residues and expressed higher in heart (Cheung *et al*., 2000). Although all of the γ subunits have highly conserved COOH terminal domains, which bind adenine nucleotides, their NH_2 termini are highly variable in both length and sequence. In HeLa cells, AMPKγ1 and AMPKγ2 mRNA were almost equally expressed, whereas AMPKγ3 expression was hardly detected. In contrast to AMPKγ2 expression, AMPKγ1 expression was not induced by the treatment of palmitic acid. These results raises the possibility that γ2-containing AMPK complex is dominant under membrane lipid saturation, and has higher or specific affinity to the upstream kinase(s). It is also possible that AMPKγ2 itself activates the upstream kinase(s).

So far, one report has shown the connection between IRE1 and AMPK. Meares *et al*. reported that Nitric oxide (NO) is a potent activator of AMPK, and this activation is dependent on IRE1. Furthermore, the known AMPK kinases described above are not required for the activation by NO. Although they didn't mention whether XBP1 is required for the activation, they showed that the RNase activity of IRE1 participates in AMPK activation in response to nitrosative stress. Thus, membrane lipid saturation- and NO- induced AMPK activation may be mediated by a common mechanism.

As a downstream of AMPK activation, I found that SCD1 expression is

induced in both mRNA and protein levels. Promoter regions of SCD1 genes have been characterized in various species including mice and human. In addition, numerous transcription factors and co-factors bind to the SCD1 promoter suggesting a fine regulation of SCD1 expression. These include SREBP-1c, LXR, PPAR-α、C/EBP−α and PGC1α (Mauvoisin and Mounier, 2011). Among them, PGC1α is reported to be positively regulated by AMPK. PGC1α is a master regulator of mitochondrial biogenesis and coordinately activates expression of metabolism-related genes (Lin *et al.*, 2005). AMPK directly phosphorylates PGC1α, which has been proposed to cause activation of its own transcription via positive feedback loop (Jager *et al*., 2007). An alternative mechanism by which AMPK has been proposed to activate PGC1α is through promotion of its deacetylation by SIRT1 (Canto *et al*., 2010). I preliminarily observed that palmitic acid treatment induced the expression of PGC1α mRNA in HeLa cells, raising the possibility that SCD1 mRNA induction by membrane lipid saturation is due to PGC1α activation. Post-transcriptional regulation of SCD1 expression is also reported (Kato *et al.*, 2006). The degradation of SCD1 protein is known to be rapid (half-time of ~5 hours), and there is an ubiquitin-proteasome-dependent pathway for SCD1 degradation. Since IRE1 knockdown suppressed up-regulation of SCD1 protein level more potently than its mRNA level, IRE1-dependent SCD1 up-regulation under membrane lipid saturation may be also caused by stabilization of SCD1 protein.

XBP1 is a major downstream effector of IRE1 and a key regulator of the mammalian UPR. In contrast, the present study revealed that IRE1-dependent AMPK activation is entirely independent of XBP1. I also showed that IRE1-dependent

up-regulation of AMPKγ2 is independent of XBP1 but requires RNase activity of IRE1. The main function of IRE1 RNase is to cleave two specific sites in the mRNA encoding XBP1, which leads to translation of active XBP1 through removal of a regulatory intron. Recently, IRE1 has been reported to cleave a subset of mRNA that is associated with the ER membrane (Maurel *et al*., 2014). In addition to mRNAs, recent studies have also identified several precursors of miRNA (pre-miRNA) to be cleaved by IRE1 RNase (Upton *et al*., 2012; Lerner *et al*., 2012). Upton *et al.* have recently proposed a pro-apoptotic pathway that is dependent on IRE1 RNase activity toward miRNA precursors. They found that IRE1-mediated cleavage of miRNAs that normally repress the translation of caspase2 mRNA and their cleavage leads to increased expression of this initiator protease. By uising bioinformatic analysis of the 3'UTR of AMPKγ2, I identified several miRNA candidates that regulate AMPKγ2 expression. I measured the expression of several candidate miRNAs by qRT-PCR, however, I couldn't detect significant change so far (Figure 30). Nevertheless, it remains possible that up-regulation of AMPKγ2 mRNA is due to IRE1-dependent degradation of some other miRNAs.

The finding that AMPK is activated by palmitic acid or SCD1 inhibitor, but not tunicamycin, suggests that IRE1 is differently activated in response to membrane lipid saturation and unfolded protein accumulation. Consistent with this, our laboratory previously demonstrated that higher order oligomerization of IRE1, which occurs upon treatment of canonical ER stressors, does not occur upon palmitic acid treatment (Kitai *et al*., 2013). Since the stability of AMPKγ2 mRNA was elevated by membrane lipid

saturation but not by unfolded protein accumulation, and AMPKγ2 up-regulation was required for RNase activity of IRE1, I speculate that the difference of IRE1 activation leads to change in the substrate specificity of IRE1 RNase. Now we are searching for the binding proteins and/or phosphorylation sites of IRE1 that are specifically detected under membrane lipid saturation.

Lipid-induced UPR has received considerable attention recently because of its association with metabolic diseases. For example, ER stress and sustained UPR signaling have been well documented in affected tissues in type 2 diabetes (Ozcan *et al.*, 2004; Ozcan *et al.*, 2006; Puri *et al*., 2008; Gregor *et al*., 2009). Thus, although the pathological aspects of UPR activation are well investigated, the physiological significance of lipid-induced UPR remains to be elucidated. On the other hand, there are substantial evidences suggesting that AMPK is dysregulated in experimental animals and humans with metabolic syndrome or type 2 diabetes and that activation of AMPK exhibits multiple protective effects, including inhibition of insulin resistance, and reduces the risk of developing type 2 diabetes (Bandyopadhyay *et al.*, 2006; Xu *et al.*, 2012). In fact, metformin, an activator of AMPK, is widely used as an anti-diabetic drug (Nathan *et al*., 2009; Rena *et al.*, 2013). From these reports and my results, I speculate that AMPK is activated through lipid-induced UPR as an adaptive response, but in chronic state, AMPK is not activated any more and prolonged UPR activation impairs cellular function, which contributes to development of metabolic diseases. Although further studies using *in vivo* models are needed to fully elucidate the biological significance of IRE1-AMPK signaling, the results from the present study provide a new

aspect of the role of the UPR in metabolic diseases.

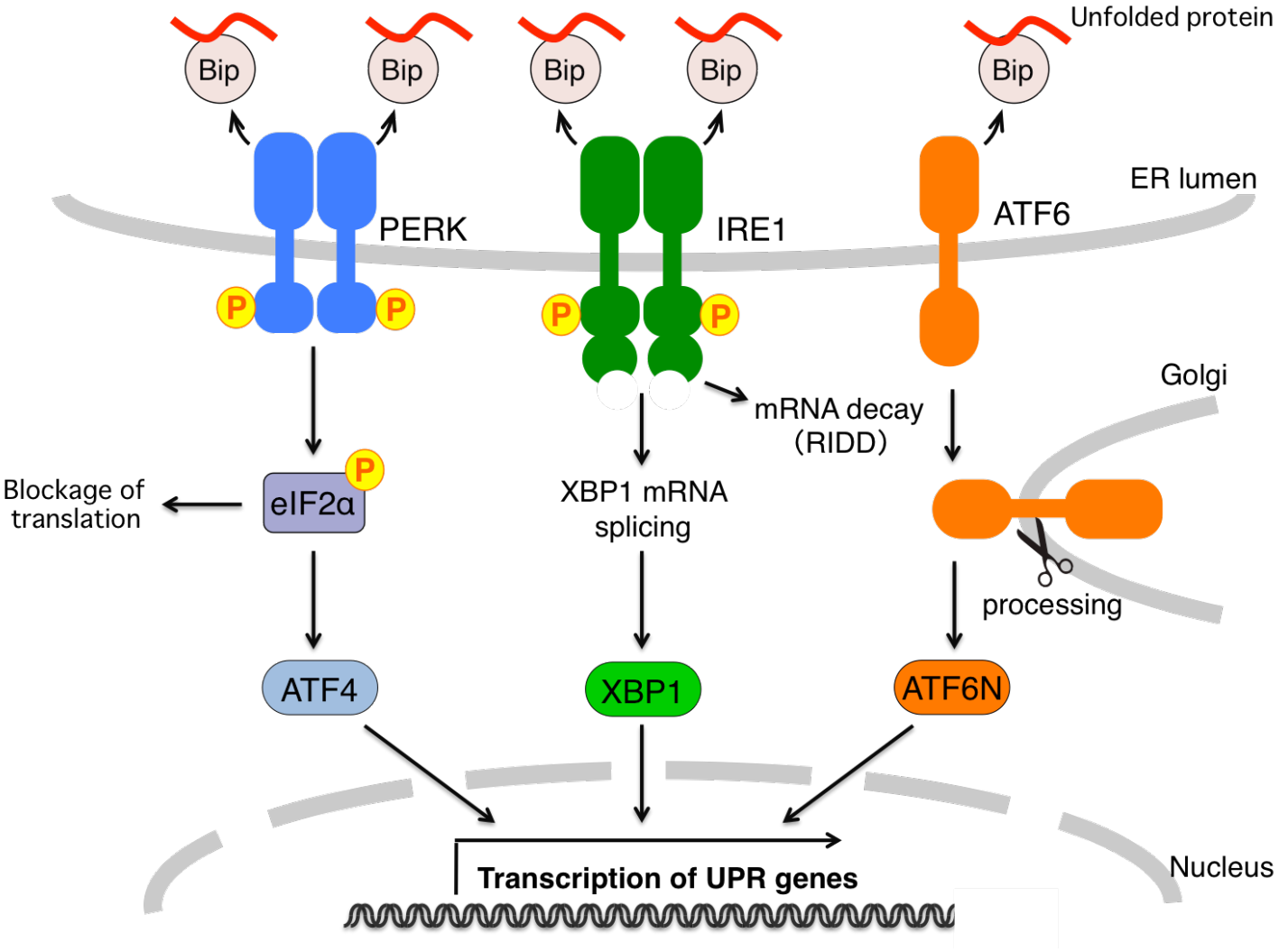

Figure 1. The unfolded protein response (UPR) pathway

In unstressed conditions, the BiP chaperone interacts with the luminal domain of the three ER transmembrane sensors, IRE1, PERK, and ATF6 to maintain them in an inactive state. Upon ER stress, BiP interacts with unfolded proteins, leading to the activation of the UPR sensors. PERK phosphorylates eIF2α to decrease global translation attenuation. Phosphorylation of eIF2α then induces the selective translation of ATF4. IRE1 cleaves the XBP1 mRNA to form the transcription factor XBP1s that induces expression of ERAD proteins and chaperones. ATF6 is proteolytically activated in the Golgi. This releases its transcriptionally active N-terminal domain. Sustained ER stress can lead to ER stress-associated cell death.

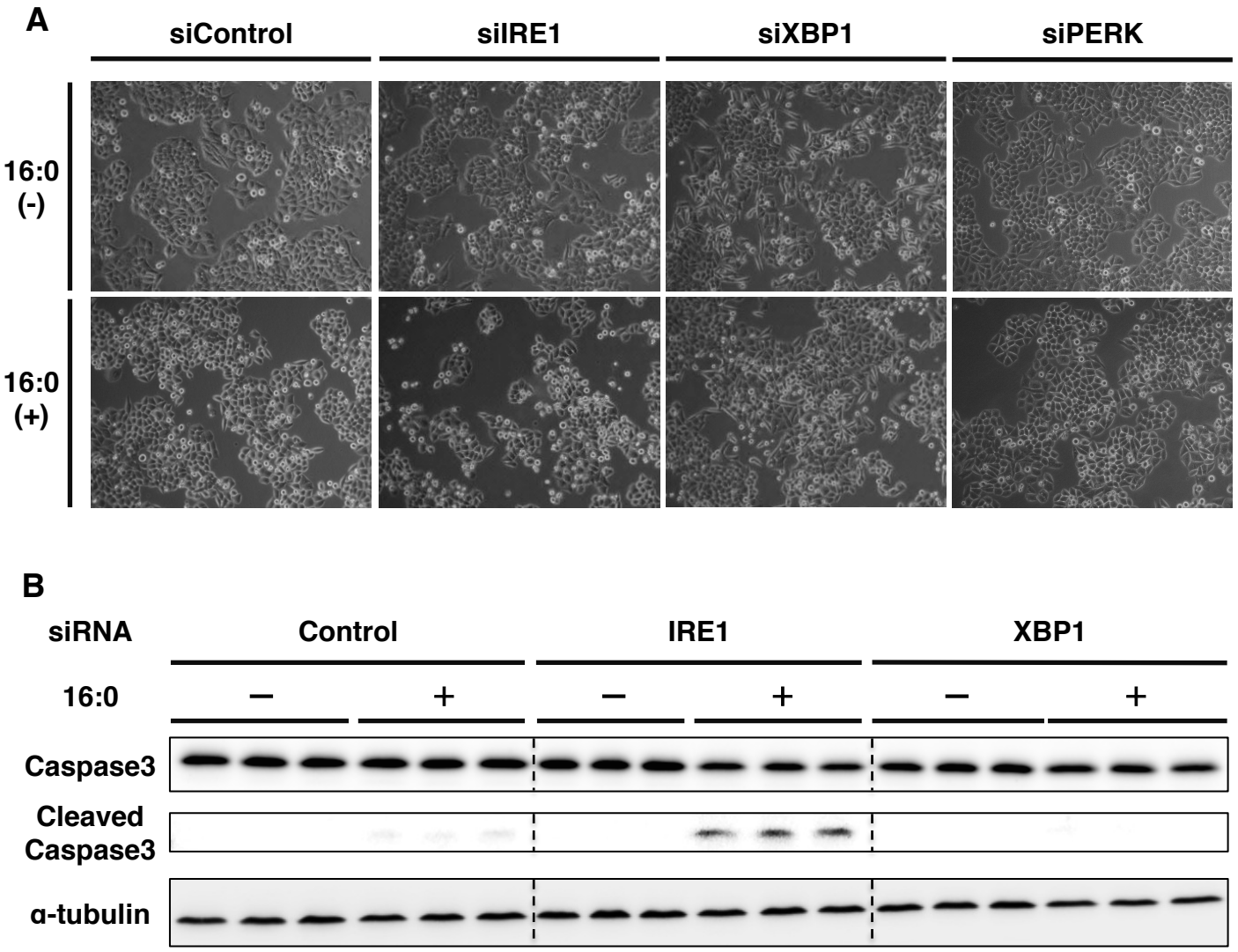

Figure 2. The effect of IRE1 knockdown on HeLa cells treated with saturated fatty acid
(**A, B**) HeLa cells were transfected with the indicated siRNAs. At 72 h after transfection, cells were treated with 16:0 (100 μM) for 12 h. (**A**) Representative photographs were taken under phase-contrast microscopy. (**B**) Whole cell lysates were subjected to immunoblot analysis using indicated antibodies. α-tubulin was used as a loading control.

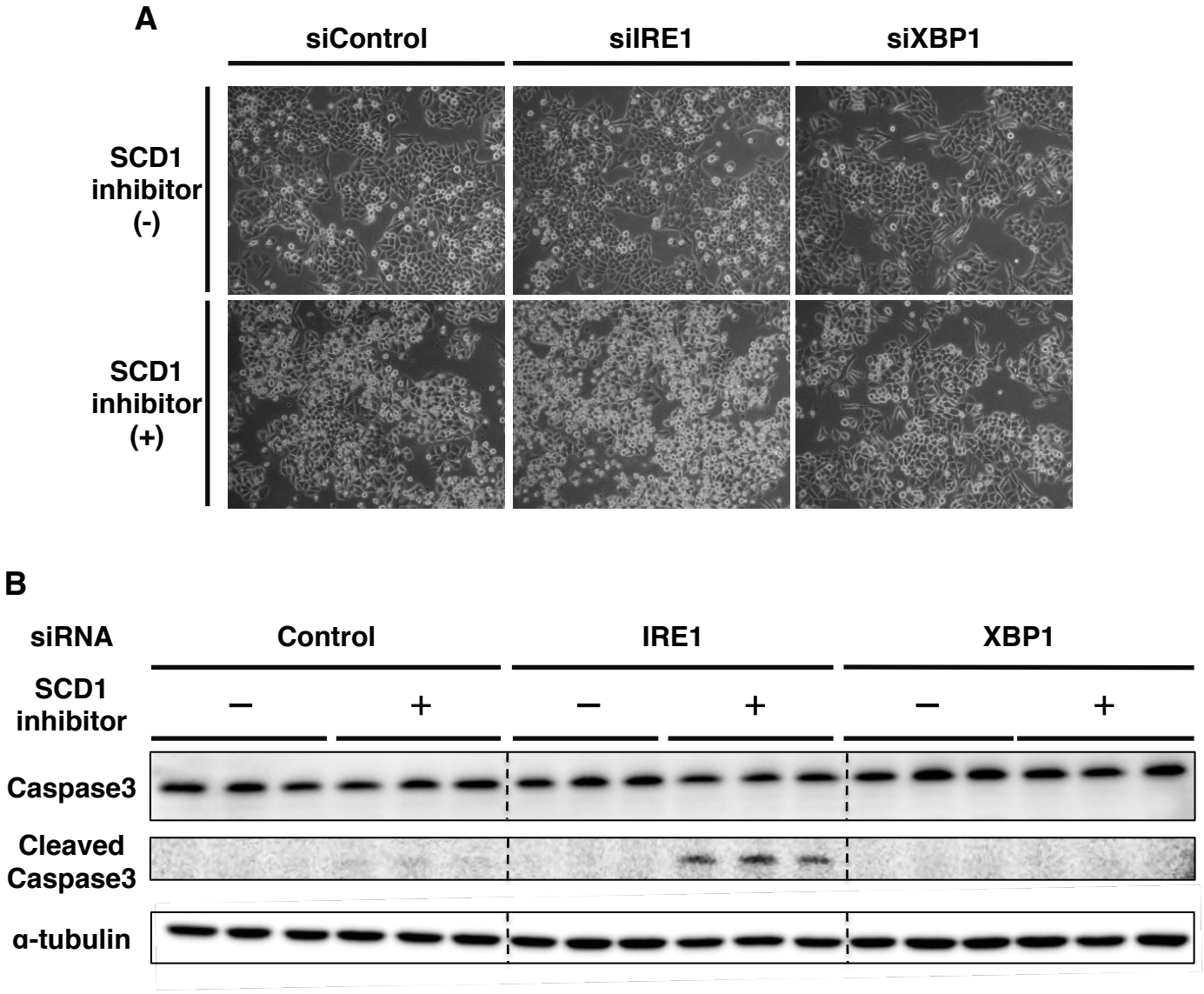

Figure 3. The effect of IRE1 knockdown on HeLa cells treated with SCD1 inhibitor

(**A, B**) HeLa cells were transfected with the indicated siRNAs. At 72 h after transfection, cells were treated with SCD1 inhibitor (5 μM) for 24 h. (**A**) Representative photographs were taken under phase-contrast microscopy. (**B**) Whole cell lysates were subjected to immunoblot analysis using indicated antibodies. α-tubulin was used as a loading control.

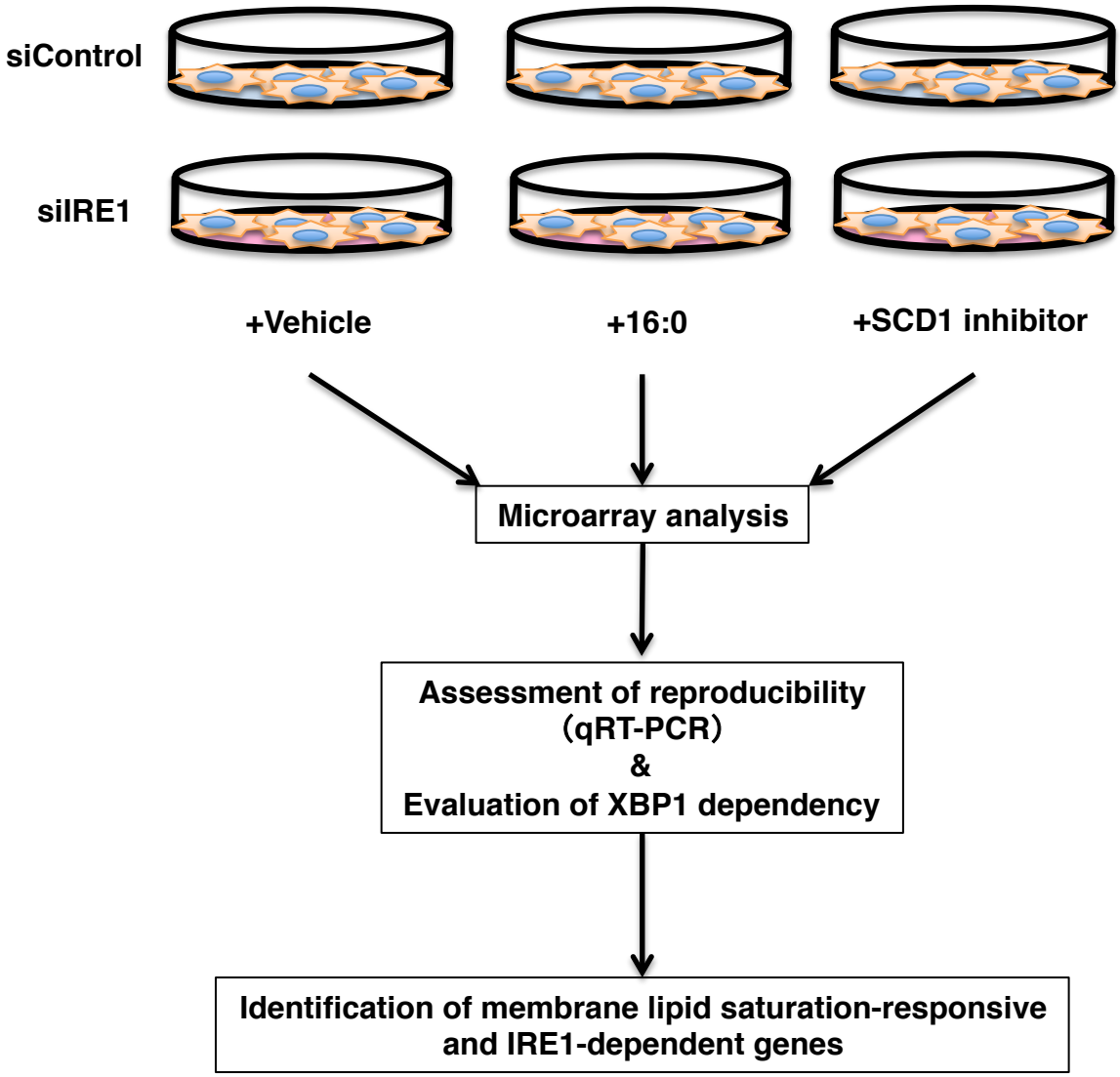

Figure 4. Strategy of identification of membrane lipid saturation-responsive and IRE1-dependent genes

HeLa cells were transfected with the indicated siRNAs. At 72 h after transfection, cells were treated with palmitic acid (100 μM) for 12 h or SCD1 inhibitor (5 μM) for 24 h.

Candidate genes were firstly picked up by microarray analysis. Then the reproducibility of the microarray results and XBP1 dependency were confirmed by quantitative real-time PCR (qRT-PCR).

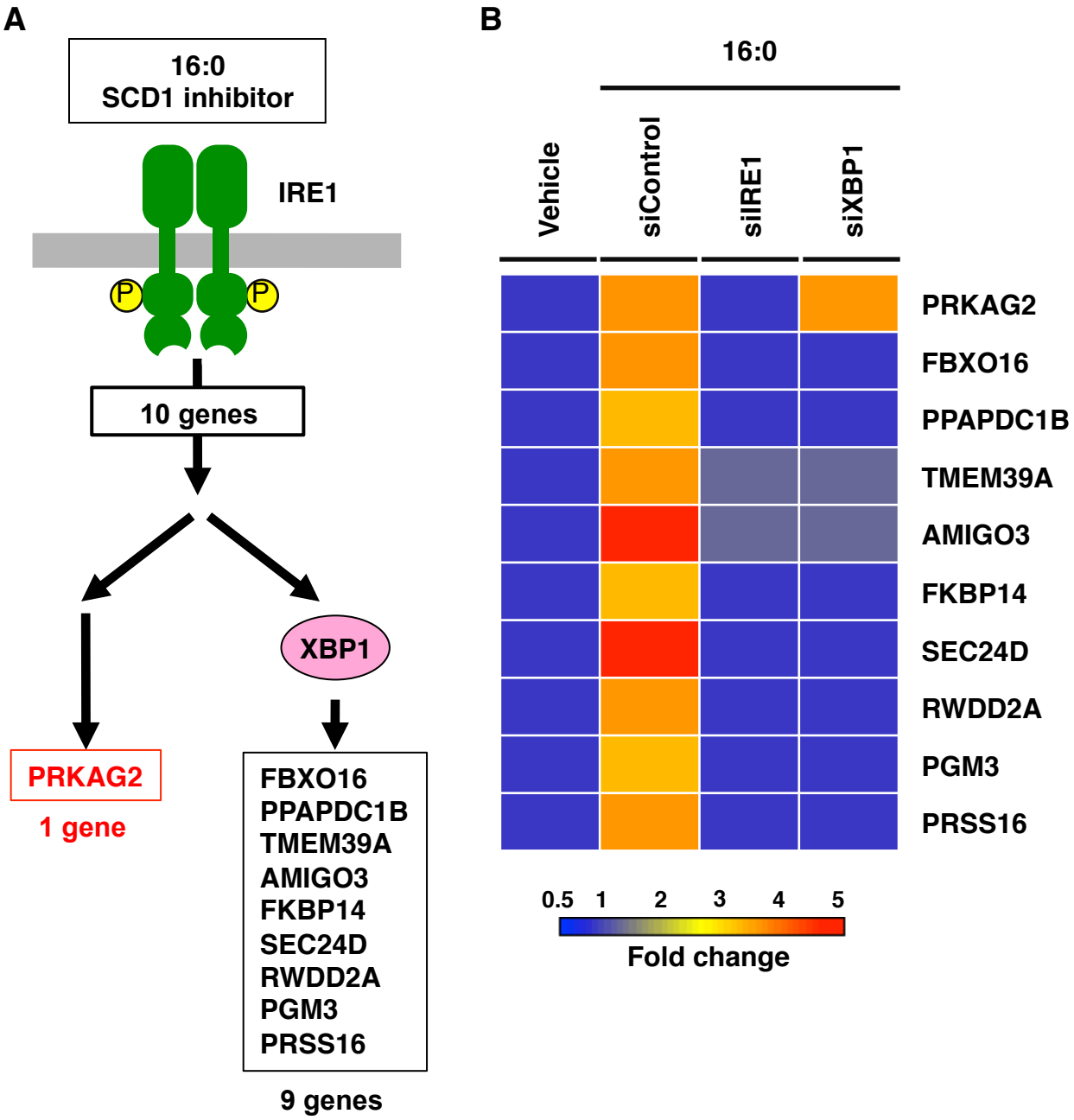

Figure 5. Summary of microarray analysis

(**A**) 10 genes were identified as membrane lipid saturation-responsive and IRE1-dependent genes. Among them, PRKAG2 is up-regulated by membrane lipid saturation independently of XBP.

(**B**) Heat maps of IRE1 dependent genes. Expression ratios calculated by quantitative real-time PCR are represented as the fold change.

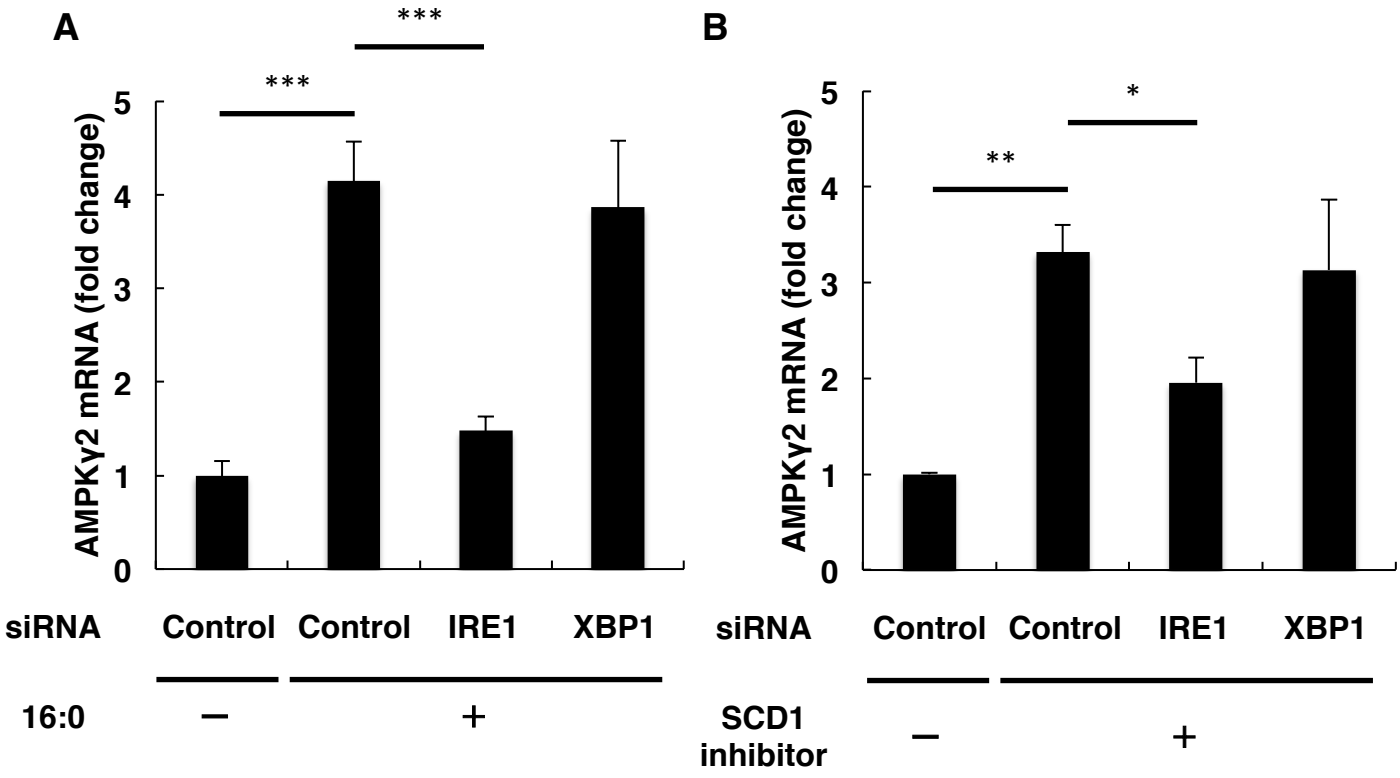

Figure 6. AMPKγ2 (PRKAG2) expression is increased by membrane lipid saturation

(**A, B**) HeLa cells were transfected with the indicated siRNAs. At 72 h after transfection, cells were treated with 16:0 (100 μM) for 12 h (**A**) or SCD1 inhibitor (5 μM) for 24 h (**B**) and then harvested. Expression of AMPKγ2 mRNA was measured by quantitative real-time PCR. The expression level of gene was normalized to expression of GAPDH gene and is represented as fold change over control siRNA transfected cells.

The data represents the mean ± SEM (n=3). *p<0.05, **<0.01, ***p<0.001.

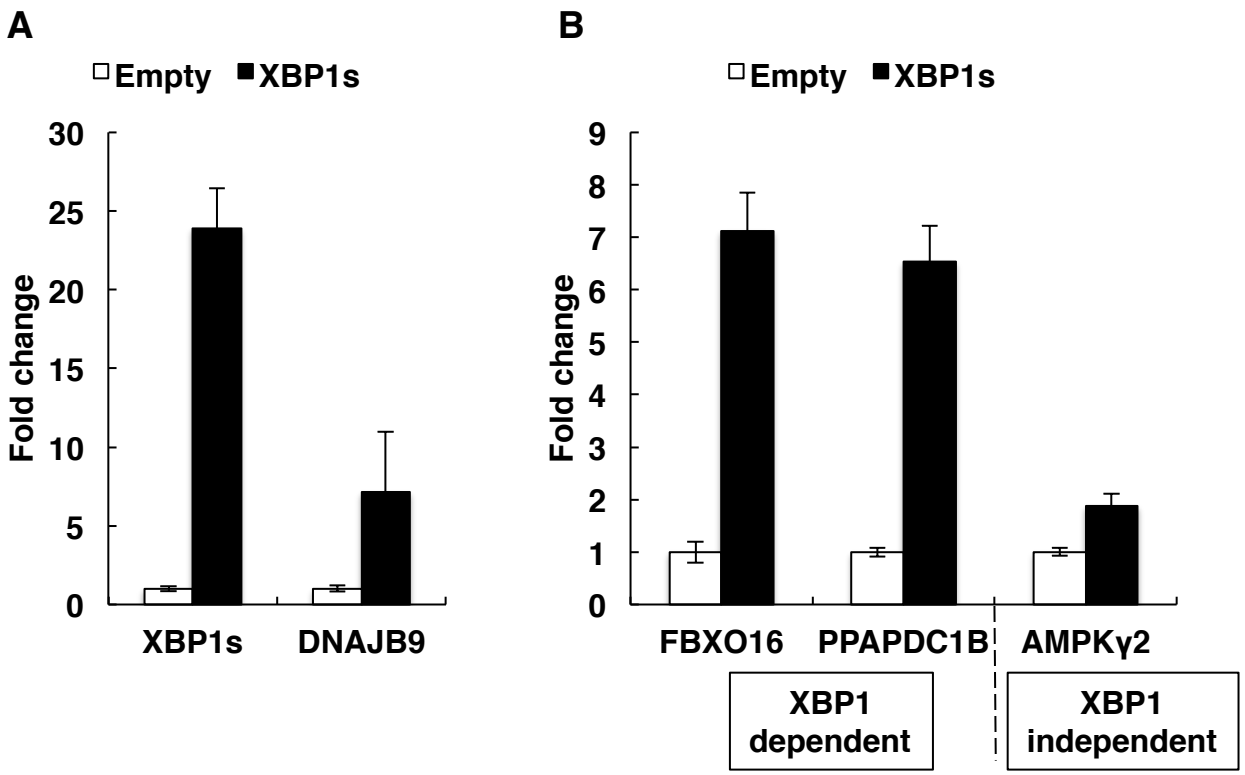

Figure 7. XBP1s does not induce AMPKγ2 expression

(**A, B**) Expression of indicated genes in HeLa cells stably expressing XBP1s was measured by quantitative real-time PCR. The expression level of gene was normalized to expression of GAPDH gene and is represented as fold change over empty vector-expressing cells.

The data represents the mean ± SEM (n=3).

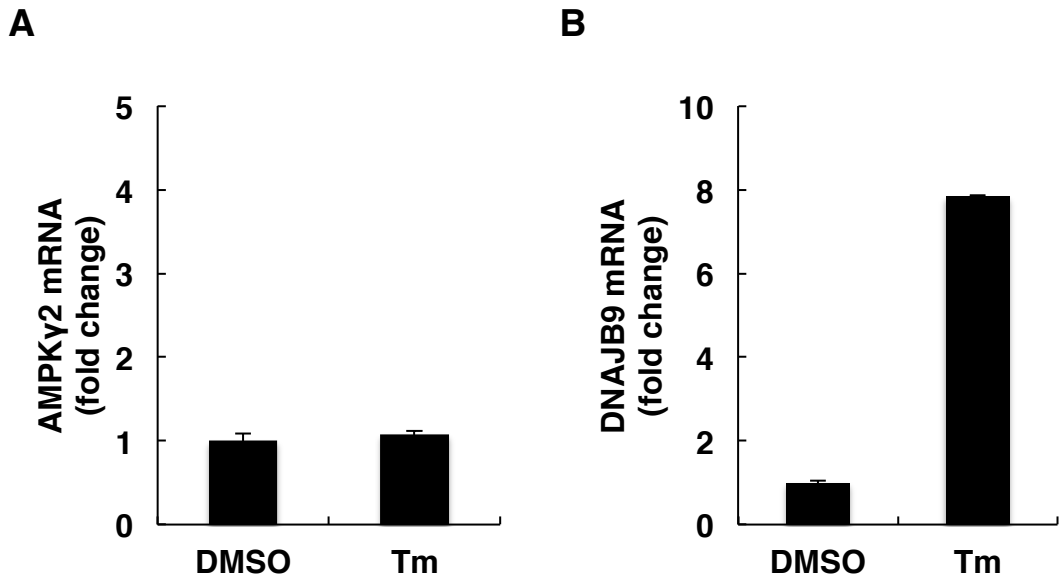

Figure 8. Tunicamycin treatment does not induce AMPKγ2 expression

(**A, B**) HeLa cells were treated with tunicamycin (2.5μg/ml) for 4 h and then harvested. Expression of AMPKγ2 (**A**) and DNAJB9 (**B**) mRNA was measured by quantitative real-time PCR. The expression level of gene was normalized to expression of GAPDH gene and is represented as fold change over control cells.

The data represents the mean ± SEM (n=3).

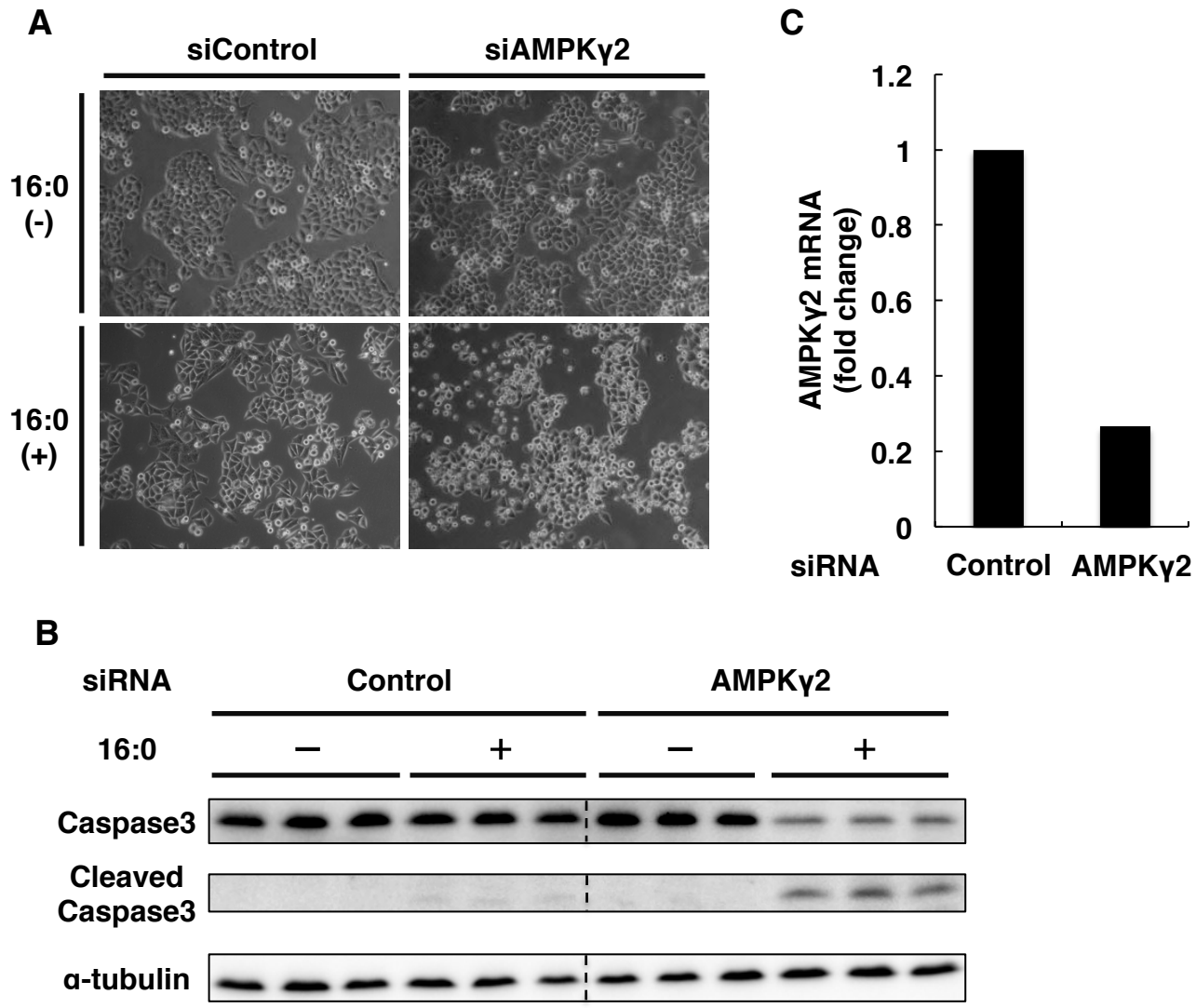

Figure 9. The effect of AMPKγ2 knockdown on HeLa cells treated with saturated fatty acid

(**A, B**) HeLa cells were transfected with the indicated siRNAs. At 72 h after transfection, cells were treated with 16:0 (100 μM) for 12 h. (**A**) Representative photographs were taken under phase-contrast microscopy. (**B**) Whole cell lysates were subjected to immunoblot analysis using indicated antibodies. α-tubulin was used as a loading control.

(**C**) HeLa cells were transfected with the indicated siRNAs. At 72 h after transfection cells were harvested. Expression of AMPKγ2 mRNA was measured by quantitative real-time PCR. The expression level of gene was normalized to expression of GAPDH gene and is represented as fold change over control siRNA transfected cells (N=3).

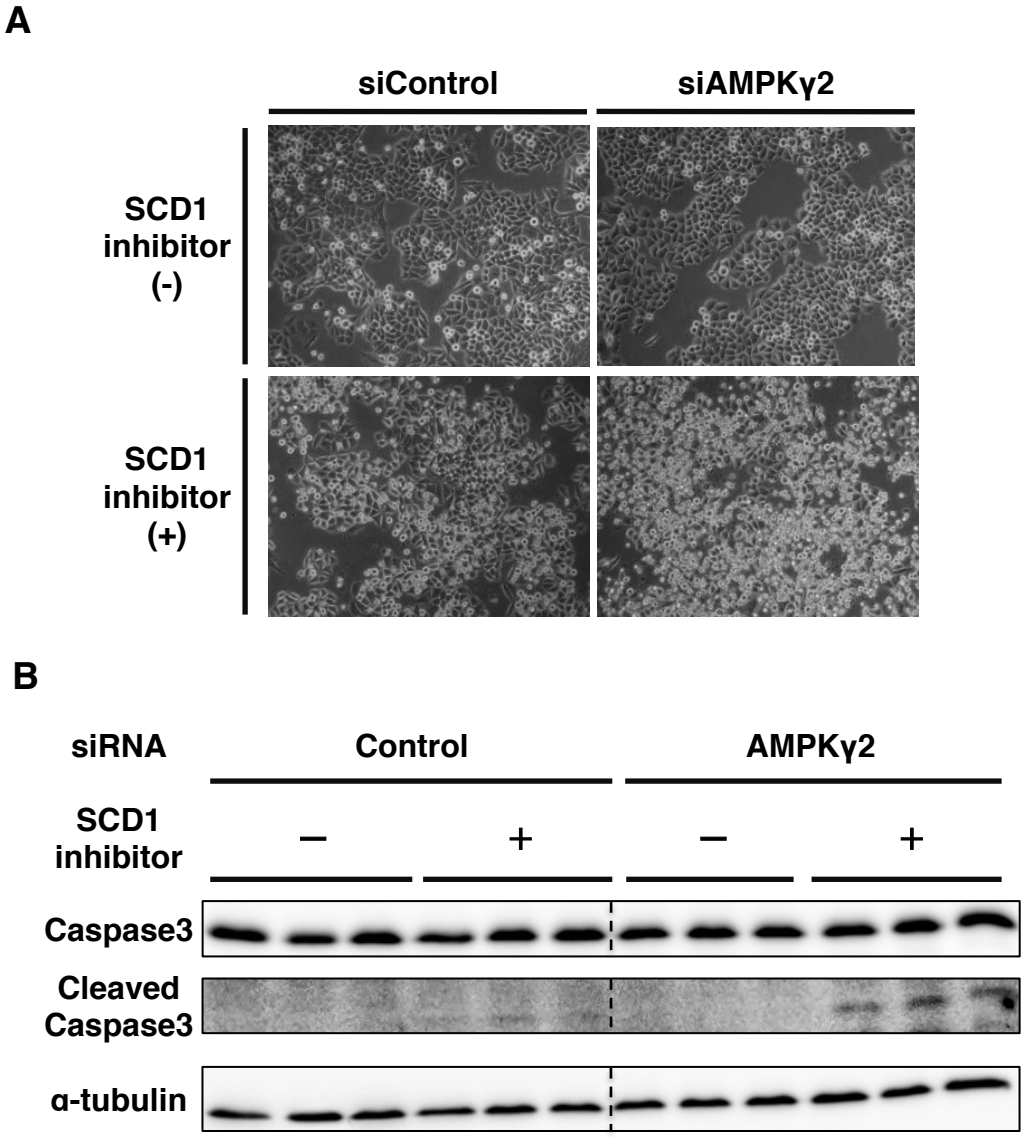

Figure 10. The effect of AMPKγ2 knockdown on HeLa cells treated with SCD1 inhibitor
(**A, B**) HeLa cells were transfected with the indicated siRNAs. At 72 h after transfection, cells were treated with SCD1 inhibitor (5 μM) for 24 h. (**A**) Representative photographs were taken under phase-contrast microscopy. (**B**) Whole cell lysates were subjected to immunoblot analysis using indicated antibodies. α-tubulin was used as a loading control.

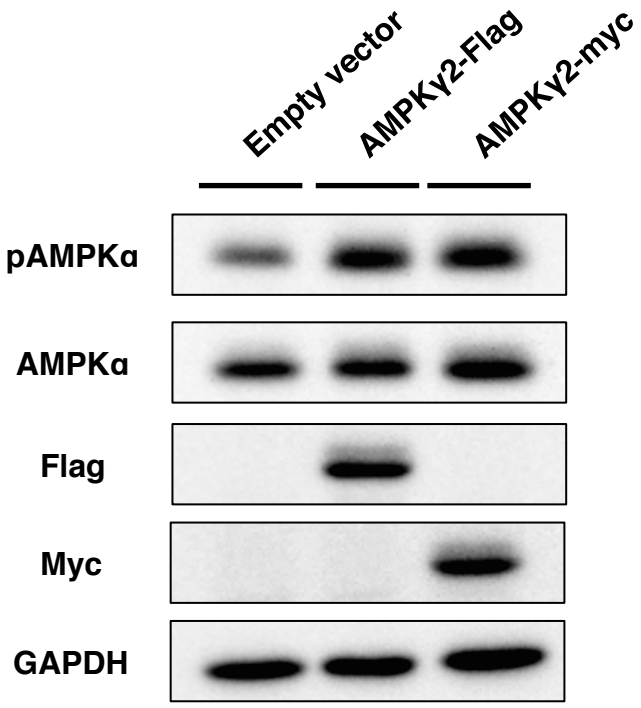

Figure 11. AMPKγ2 overexpression causes AMPKα phosphorylation

HeLa cells were transfected with the indicated plasmids. At 24 h after transfection, cells were harvested. Whole cell lysates were subjected to immunoblot analysis using indicated antibodies. GAPDH was used as a loading control. pAMPKα, phosphorylated AMPKα.

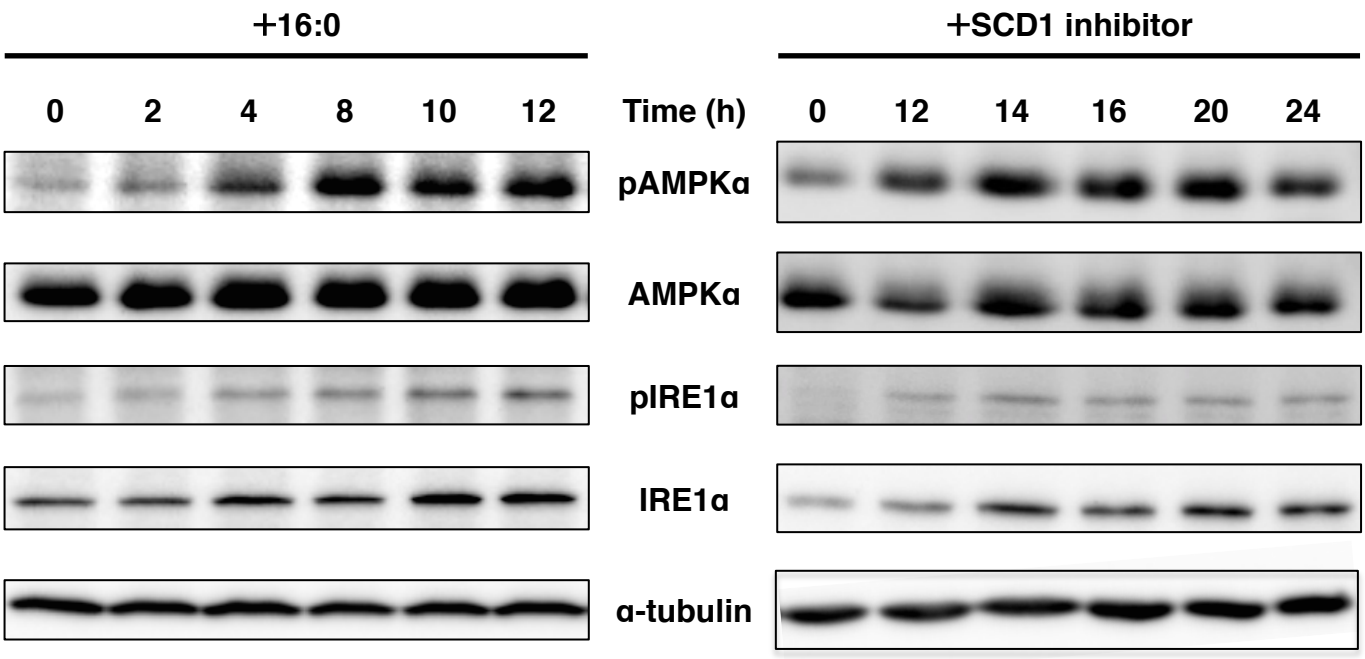

Figure 12. AMPKα is phosphorylated by membrane lipid saturation

HeLa cells were treated with 16:0 (100 μM) or SCD1 inhibitor (5 μM) for indicated duration and then harvested. Whole cell lysates were subjected to immunoblot analysis using indicated antibodies. α-tubulin was used as a loading control. pAMPKα, phosphorylated AMPKα; pIRE1α, phosphorylated IRE1α.

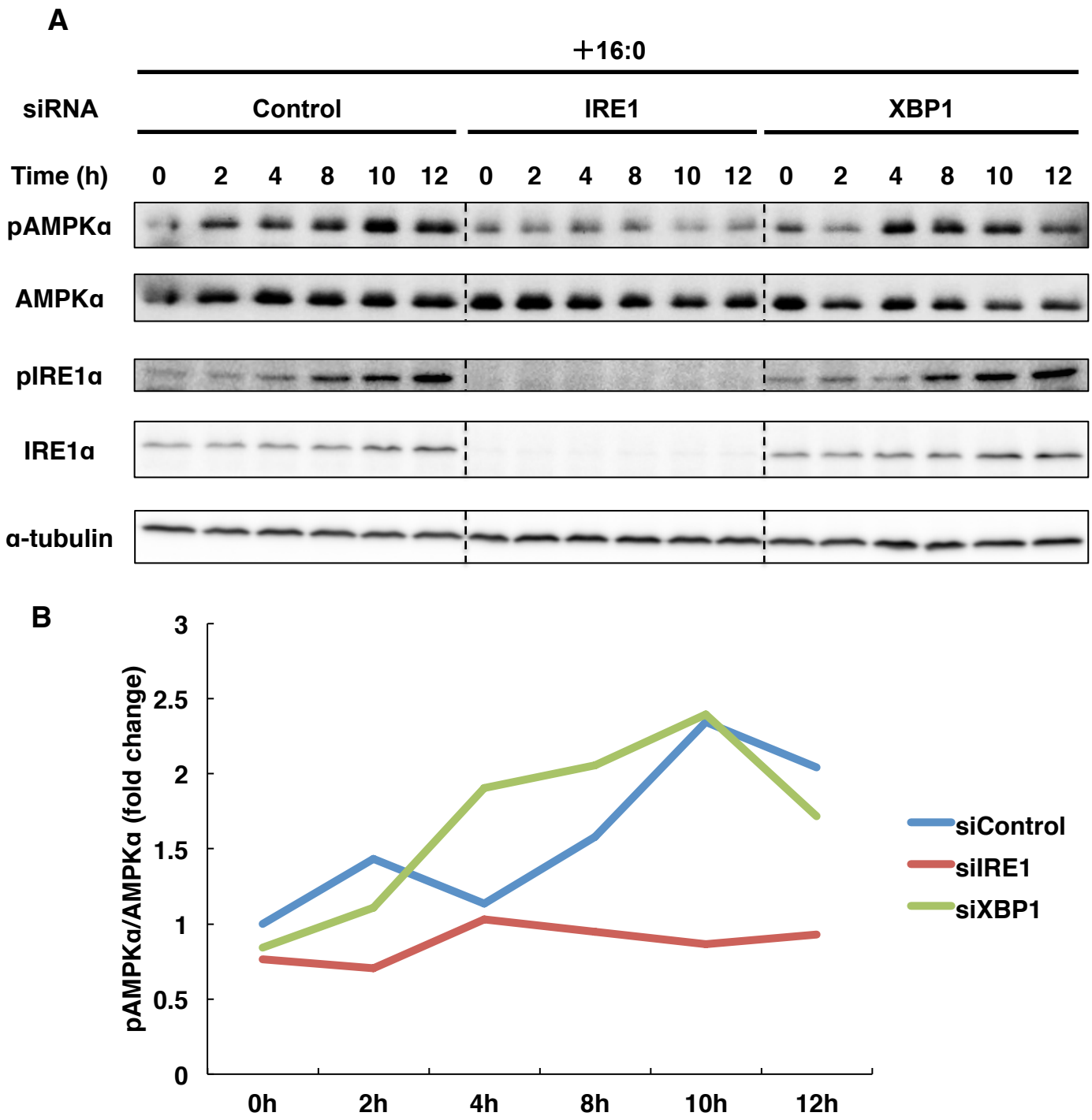

Figure 13. AMPKα phosphorylation by palmitic acid is IRE1 dependent

(**A, B**) HeLa cells were transfected with the indicated siRNAs. At 72 h after transfection, cells were treated with 16:0 (100 μM) for indicated duration and then harvested. (**A**) Whole cell lysates were subjected to immunoblot analysis using indicated antibodies. α-tubulin was used as a loading control. pAMPKα, phosphorylated AMPKα; pIRE1α, phosphorylated IRE1α. (**B**) The graph shows the ratio of phosphorylated/total AMPKα at each time point.

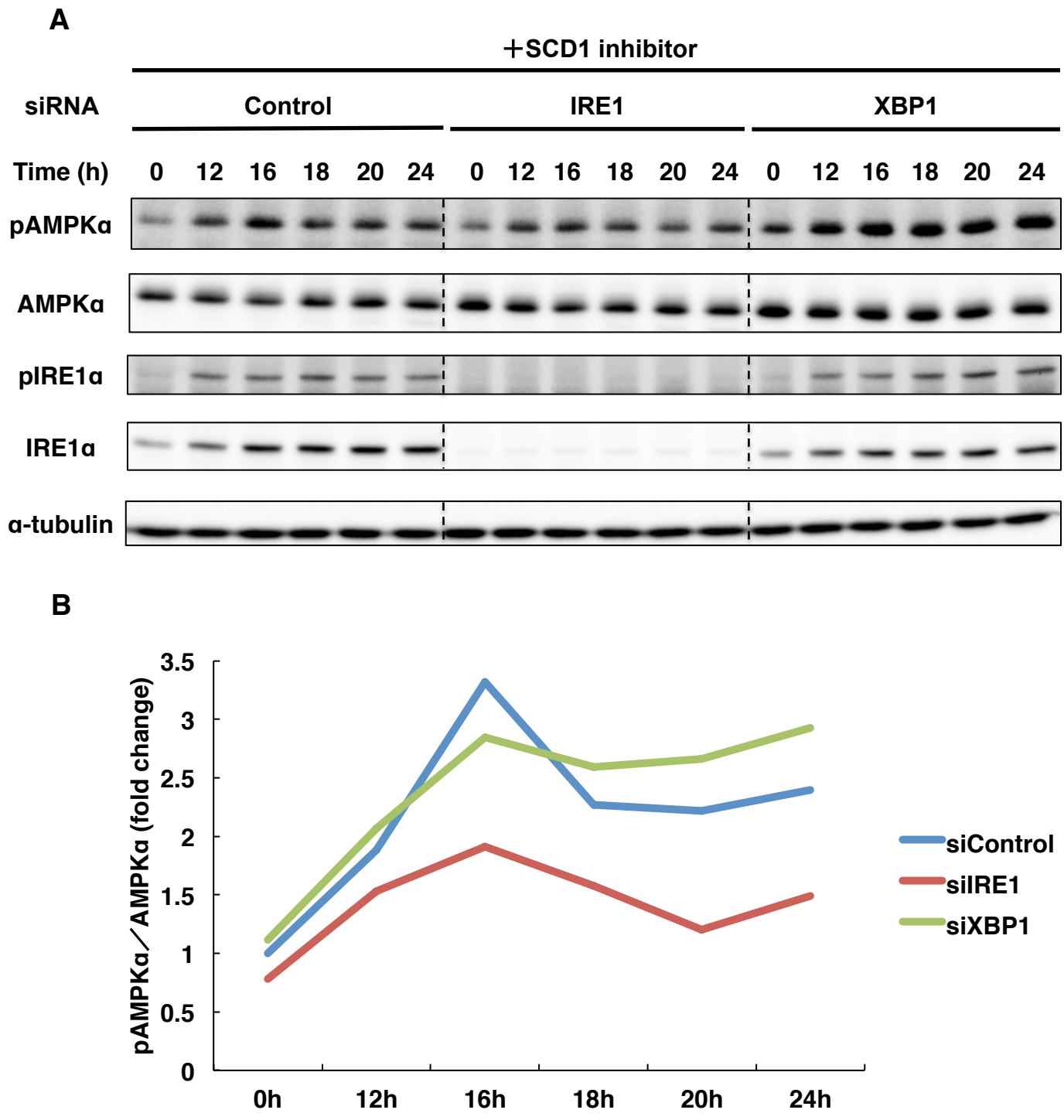

Figure 14. AMPKα phosphorylation by SCD1 inhibitor is IRE1 dependent

(**A, B**) HeLa cells were transfected with the indicated siRNAs. At 72 h after transfection, cells were treated with SCD1 inhibitor (5 μM) for indicated duration and then harvested. (**A**) Whole cell lysates were subjected to immunoblot analysis using indicated antibodies. α-tubulin was used as a loading control. pAMPKα, phosphorylated AMPKα; pIRE1α, phosphorylated IRE1α. (**B**) The graph shows the ratio of phosphorylated/total AMPKα at each time point.

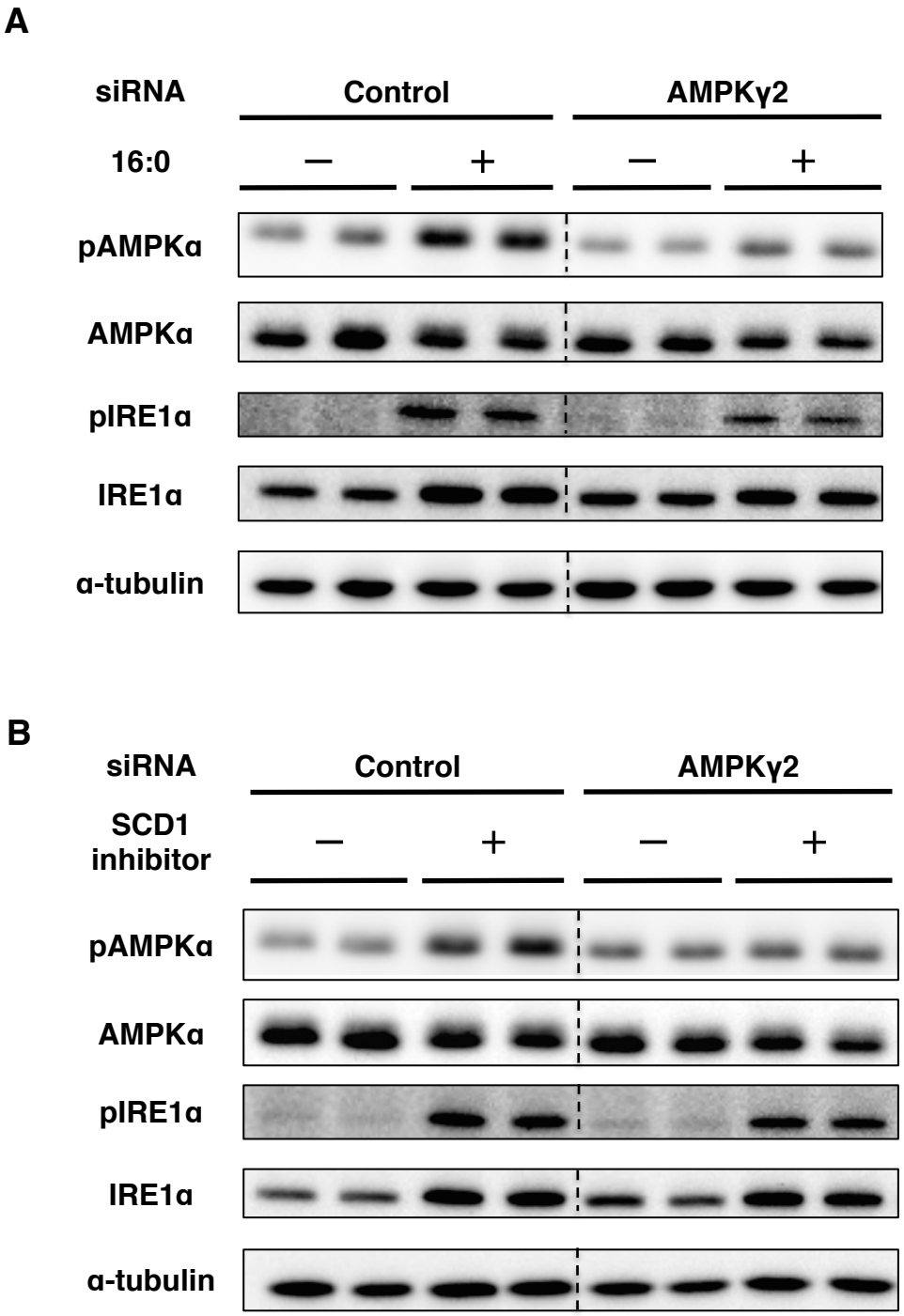

Figure 15. AMPKα phosphorylation by membrane lipid saturation is AMPKγ2 dependent
(**A, B**) HeLa cells were transfected with the indicated siRNA. At 72 h after transfection, cells were treated with 16:0 (100 μM) 12 h (**A**) or SCD1 inhibitor (5 μM) for 24 h (**B**) and then harvested. (**A**) Whole cell lysates were subjected to immunoblot analysis using indicated antibodies. α-tubulin was used as a loading control. pAMPKα, phosphorylated AMPKα; pIRE1α, phosphorylated IRE1α.

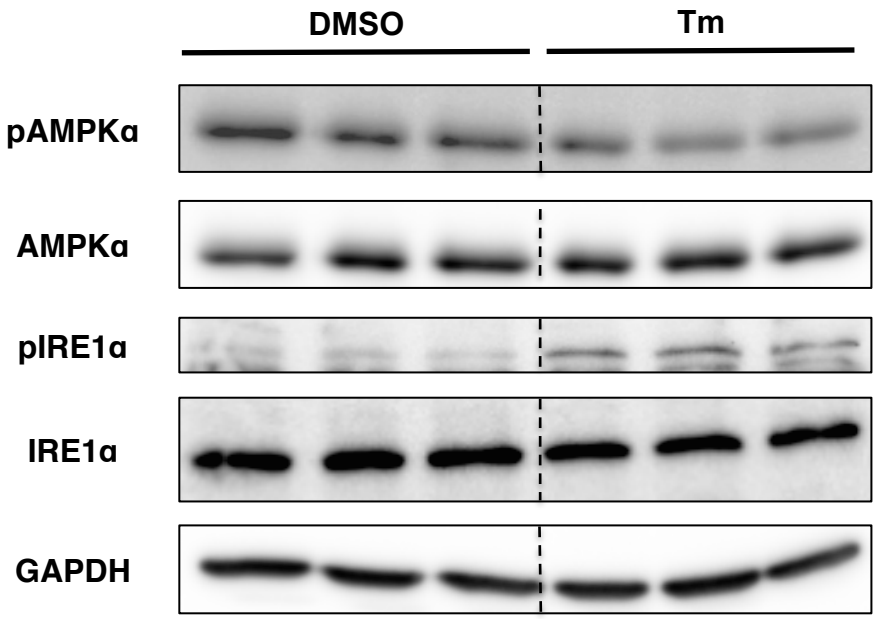

Figure 16. Tunicamycin treatment does not induce AMPKα phosphorylation
HeLa cells were treated with tunicamycin (2.5 μg/ml) for 4 h and then harvested. Whole cell lysates were subjected to immunoblot analysis using indicated antibodies. GAPDH was used as a loading control. pAMPKα, phosphorylated AMPKα; pIRE1α, phosphorylated IRE1α.

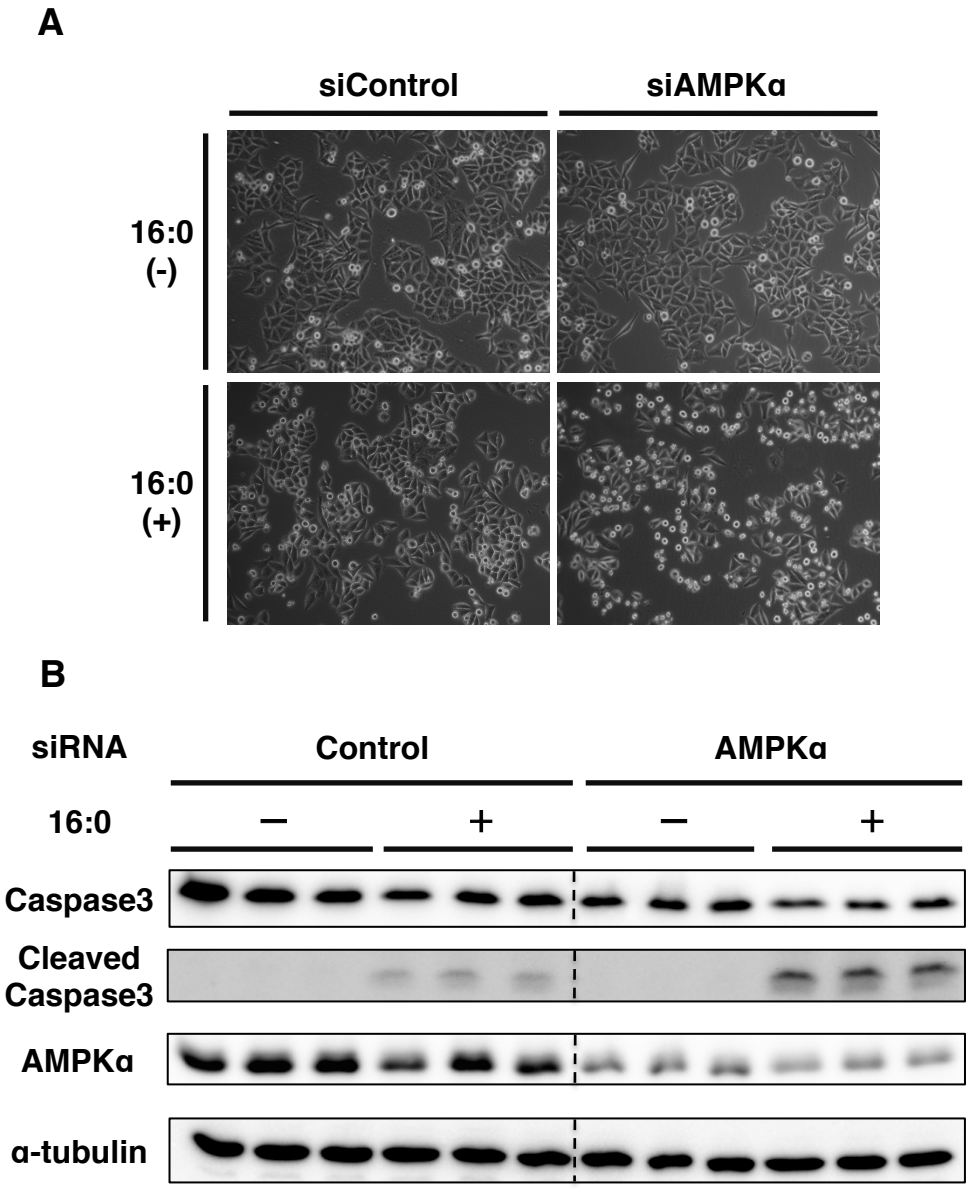

Figure 17. The effect of AMPKα knockdown on HeLa cells treated with saturated fatty acid (**A, B**) HeLa cells were transfected with the indicated siRNAs. At 72 h after transfection, cells were treated with 16:0 (100 μM) for 12 h. (**A**) Representative photographs were taken under phase-contrast microscopy. (**B**) Whole cell lysates were subjected to immunoblot analysis using indicated antibodies. α-tubulin was used as a loading control.

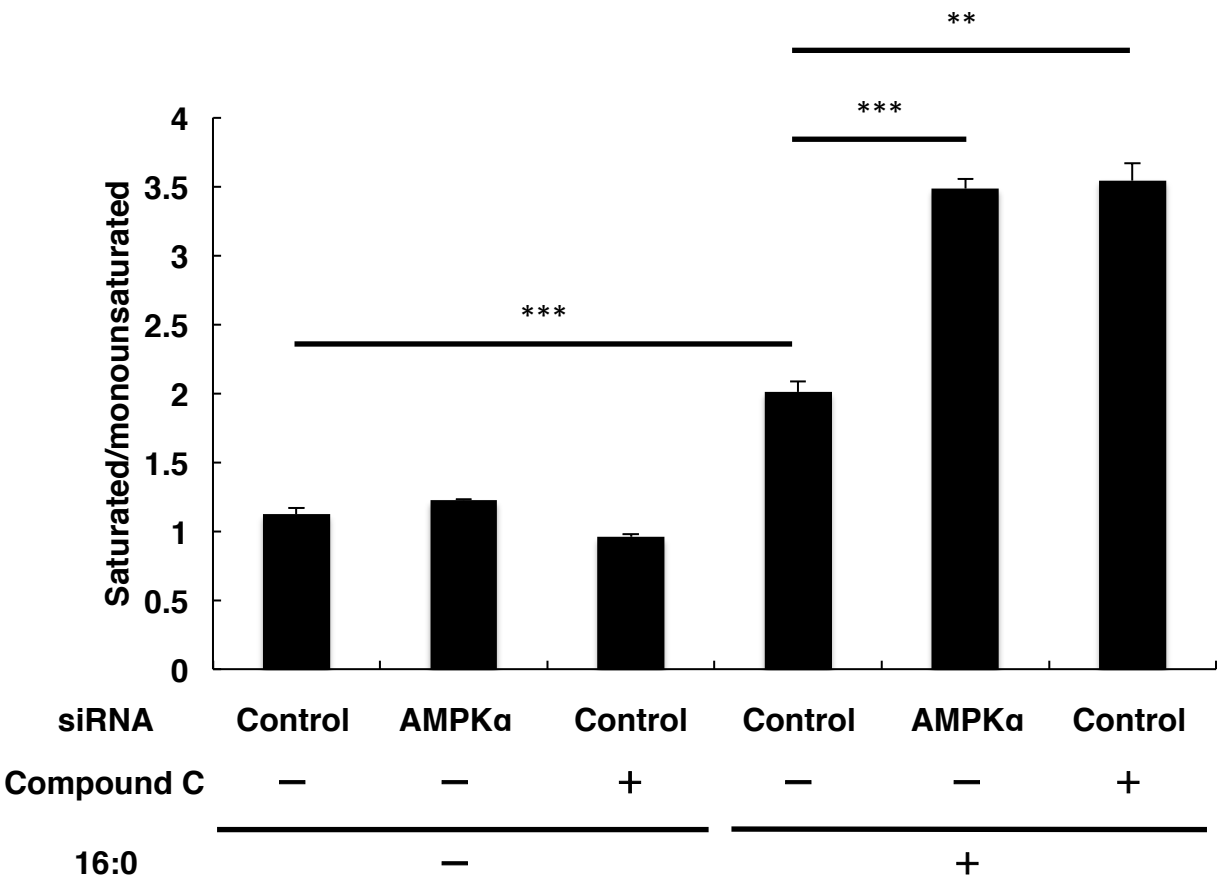

Figure 18. The ratio of saturated fatty acid to monounsaturated fatty acid is elevated by inhibition of AMPK

HeLa cells were transfected with the indicated siRNAs. At 72 h after transfection, cells were treated with 16:0 (100 μM) and Compound C (10 μM) for 12 h and then harvested. The relative abundance of fatty acid species was determined by GC-MS.

The data represents the mean ± SEM (n=3). **p<0.01, ***p<0.001.

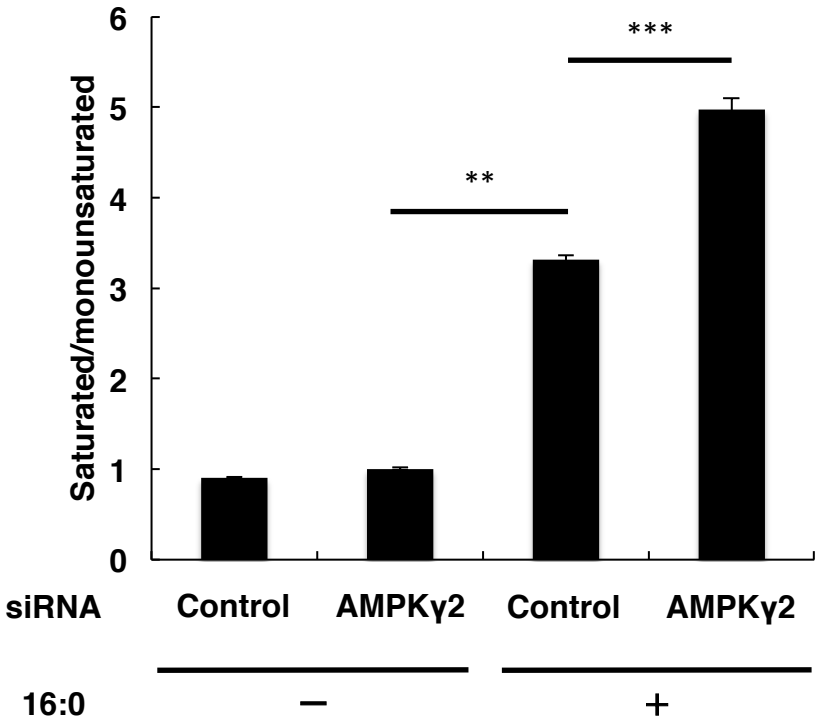

Figure 19. The ratio of saturated fatty acid to monounsaturated fatty acid is elevated by AMPKγ2 knockdown

HeLa cells were transfected with the indicated siRNAs. At 72 h after transfection, cells were treated with 16:0 (100 μM) for 12 h and then harvested. The relative abundance of fatty acid species was determined by GC-MS.

The data represents the mean ± SEM (n=3). **p<0.01, ***p<0.001.

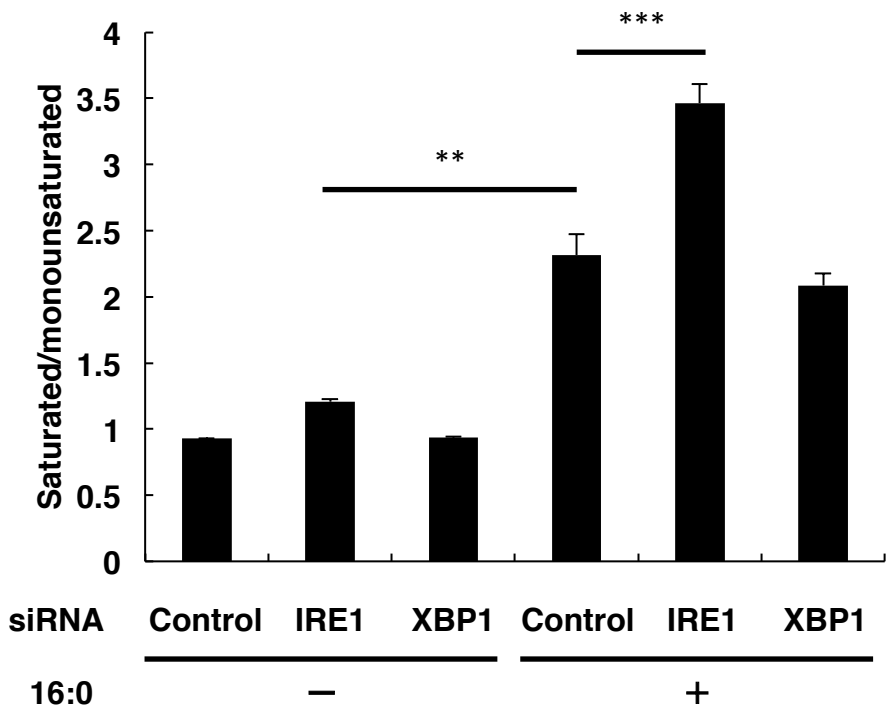

Figure 20. The ratio of saturated fatty acid to monounsaturated fatty acid is elevated by IRE1 knockdown

HeLa cells were transfected with the indicated siRNAs. At 72 h after transfection, cells were treated with 16:0 (100 μM) for 12 h and then harvested. The relative abundance of fatty acid species was determined by GC-MS.

The data represents the mean ± SEM (n=3). **p<0.01, ***p<0.001.

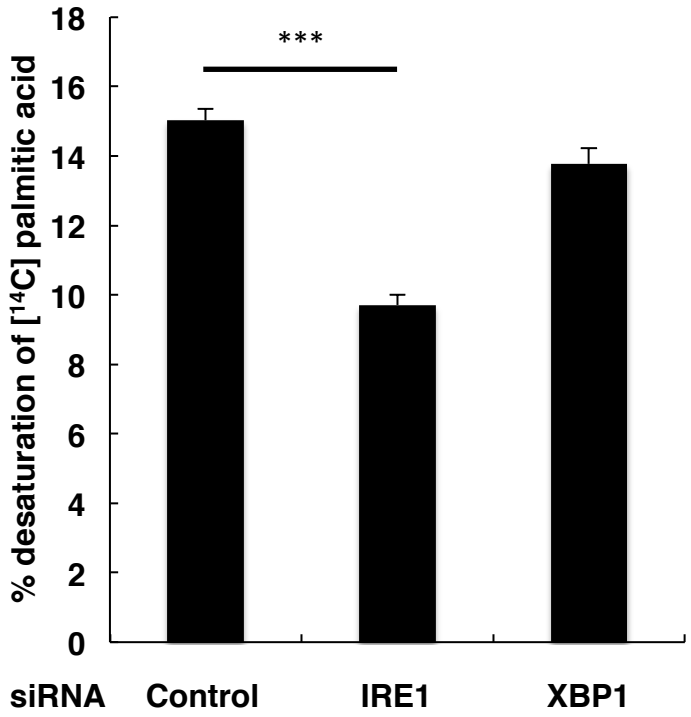

Figure 21. Desaturation of exogenous [^{14}C] palmitic acid is inhibited by IRE1 knockdown
HeLa cells were transfected with the indicated siRNAs. At 72 h after transfection, cells were treated with [^{14}C] 16:0 (100 μM) for 12 h and then harvested. Lipids were separated by TLC. The amount of desaturated [^{14}C] palmitic acid was expressed as the percentage of total radioactivity incorporated into cells.
The data represents the mean ± SEM (n=3). ***$p<0.001$.

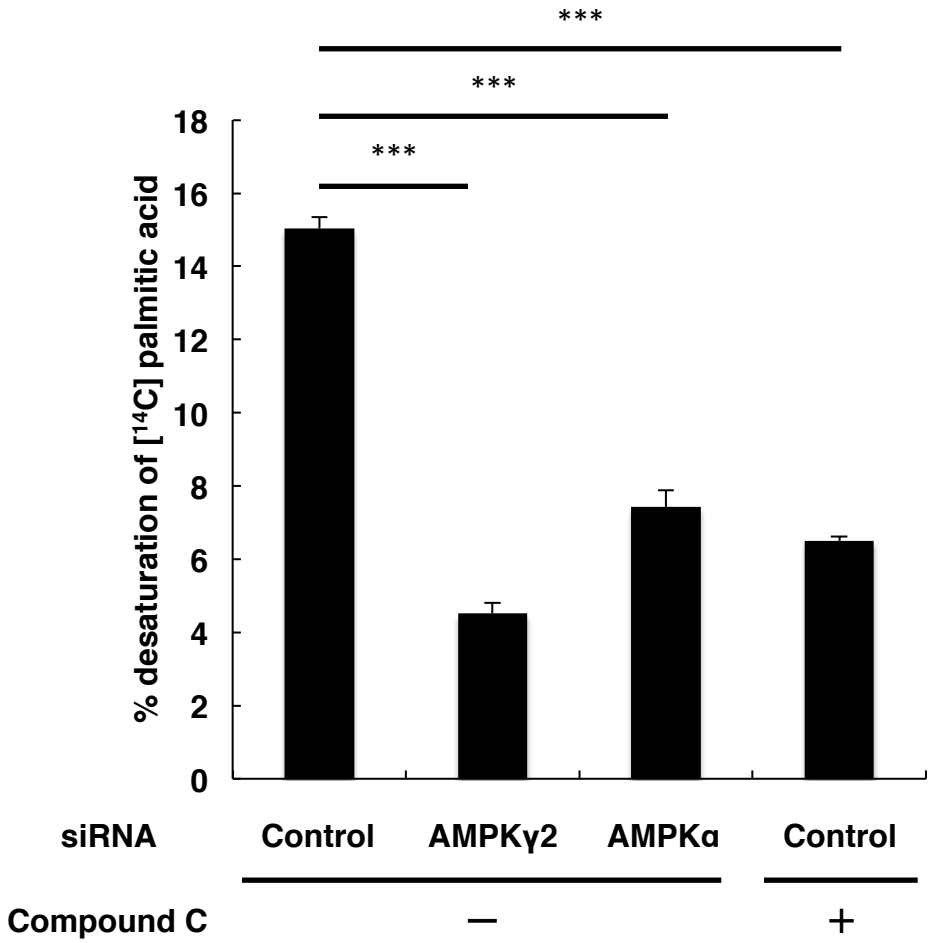

Figure 22. Desaturation of exogenous [^{14}C] palmitic acid is inhibited by inhibition of AMPK
HeLa cells were transfected with the indicated siRNAs. At 72 h after transfection, cells were treated with [^{14}C] 16:0 (100 μM) and Compound C (10 μM) for 12 h and then harvested. Lipids were separated by TLC. The amount of desaturated [^{14}C] palmitic acid was expressed as the percentage of total radioactivity incorporated into cells.
The data represents the mean ± SEM (n=3). ***$p<0.001$.

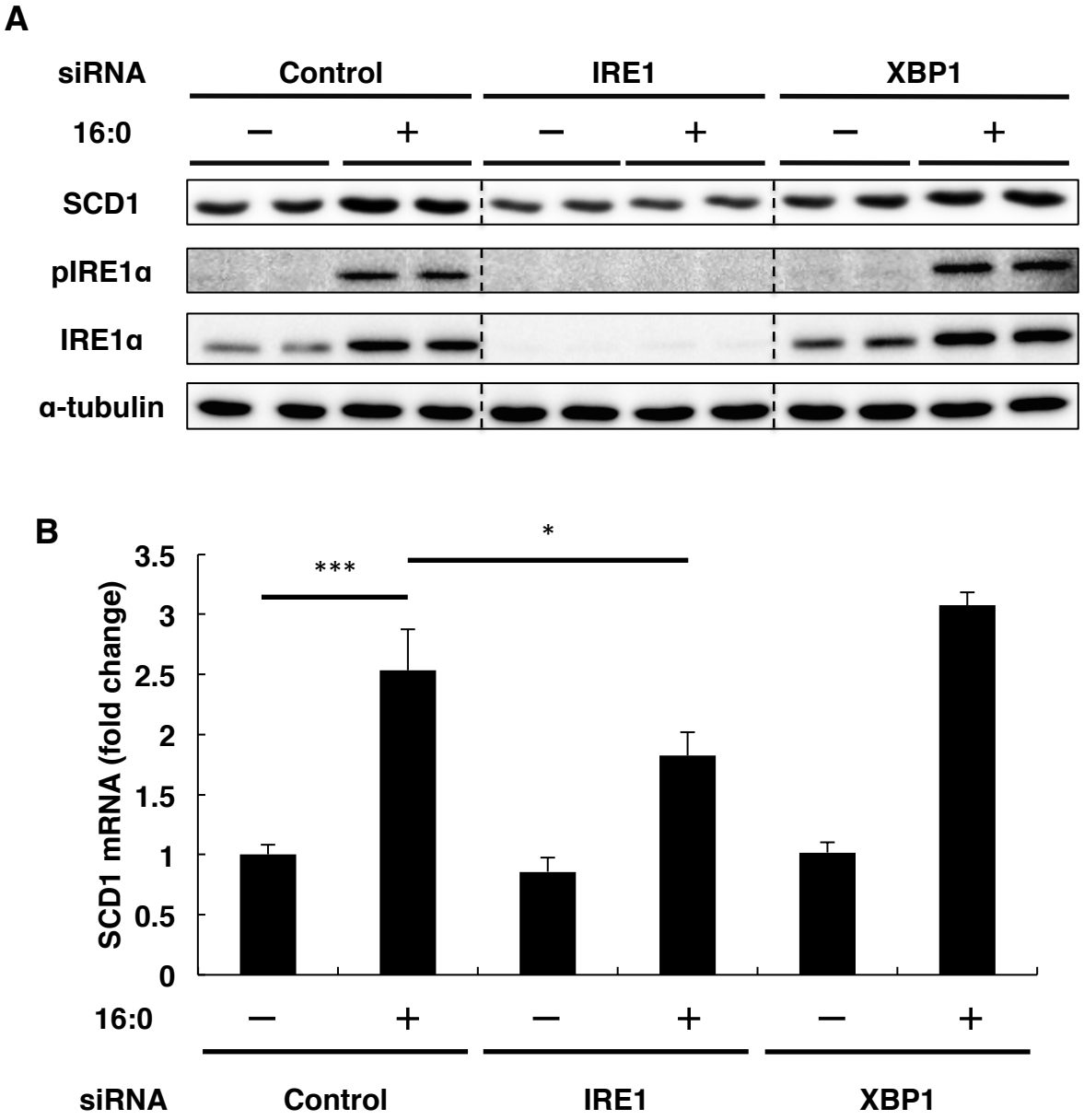

Figure 23. SCD1 expression is elevated by saturated fatty acid treatment in an IRE-dependent manner

(**A, B**) HeLa cells were transfected with the indicated siRNAs. At 72 h after transfection, cells were treated with 16:0 (100 μM) for 12 h and then harvested. (**A**) Whole cell lysates were subjected to immunoblot analysis using indicated antibodies. α-tubulin was used as a loading control. pIRE1α, phosphorylated IRE1α. (**B**) Expression of SCD1 mRNA was measured by quantitative real-time PCR. The expression level of gene was normalized to expression of GAPDH gene and is represented as fold change over control siRNA transfected cells.

The data represents the mean ± SEM (n=3). *p<0.05, ***p<0.001.

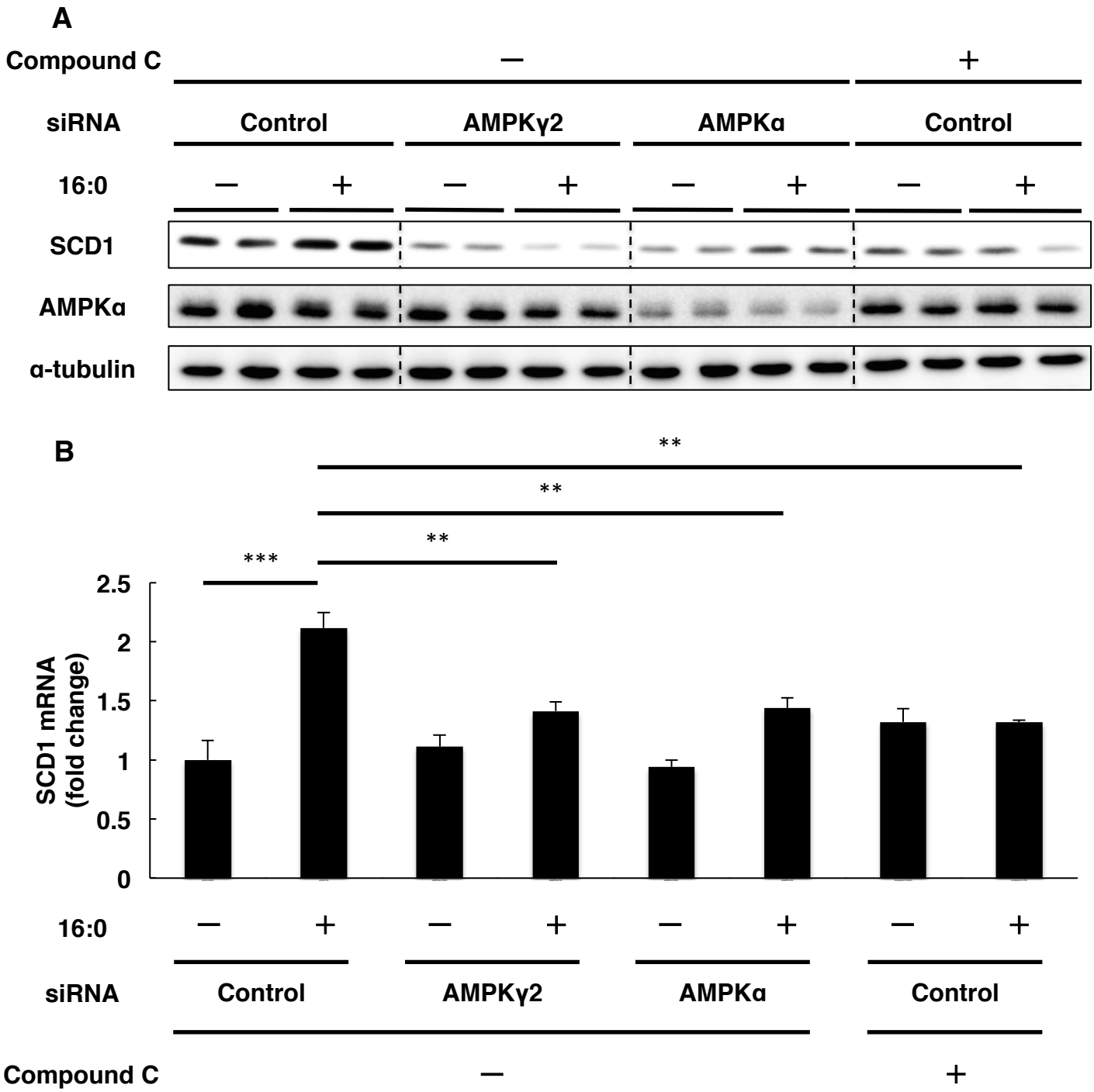

Figure 24. SCD1 expression is elevated by saturated fatty acid treatment in an AMPK-dependent manner

(**A, B**) HeLa cells were transfected with the indicated siRNAs. At 72 h after transfection, cells were treated with 16:0 (100 μM) and Compound C (10 μM) for 12 h and then harvested. (**A**) Whole cell lysates were subjected to immunoblot analysis using indicated antibodies. α-tubulin was used as a loading control. (**B**) Expression of SCD1 mRNA was measured by quantitative real-time PCR. The expression level of gene was normalized to expression of GAPDH gene and is represented as fold change over control siRNA transfected cells.

The data represents the mean ± SEM (n=3). **p<0.01, ***p<0.001.

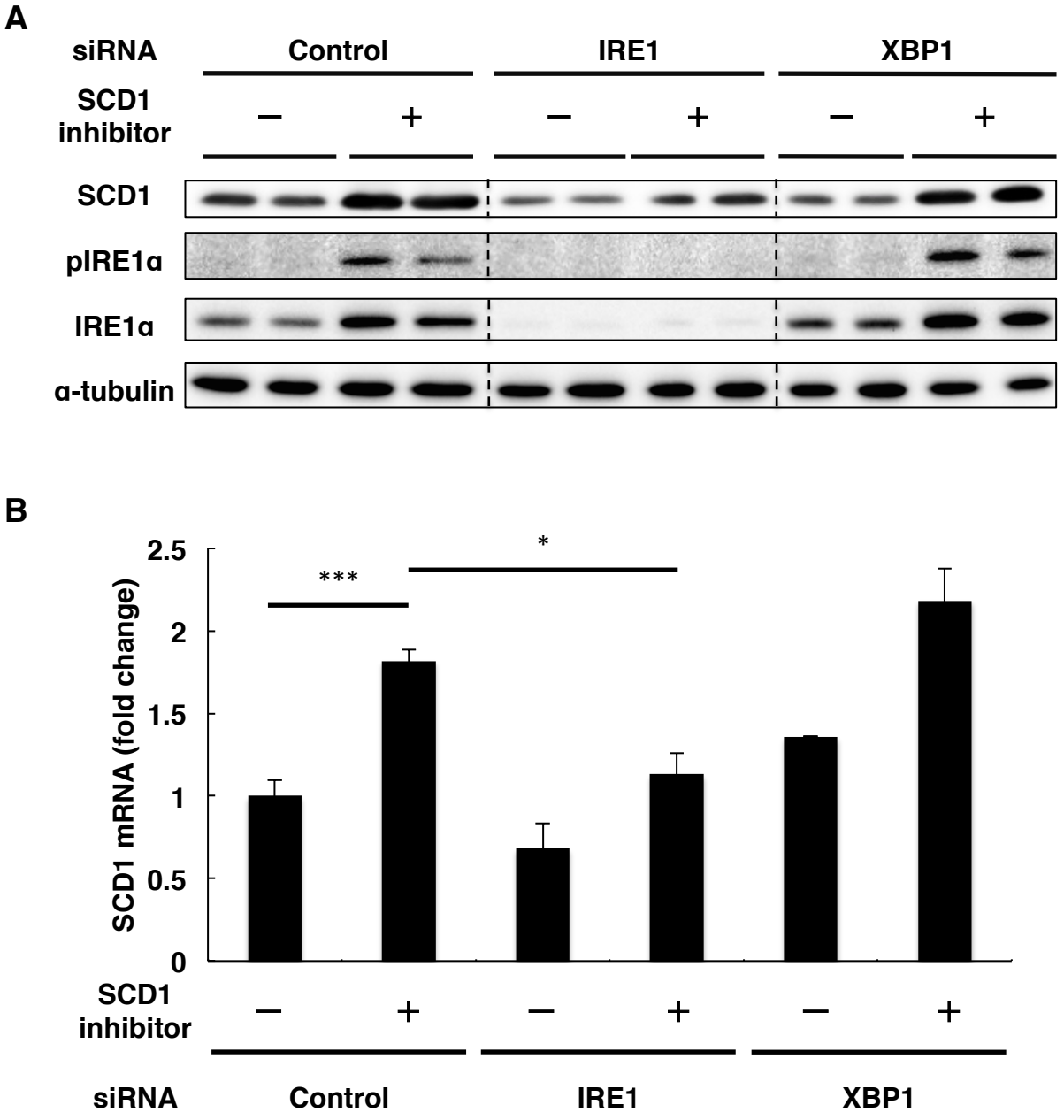

Figure 25. SCD1 expression is elevated by SCD1 inhibitor treatment in an IRE1-dependent manner

(**A, B**) HeLa cells were transfected with the indicated siRNAs. At 72 h after transfection, cells were treated with SCD1 inhibitor (5 μM) for 24 h and then harvested. (**A**) Whole cell lysates were subjected to immunoblot analysis using indicated antibodies. α-tubulin was used as a loading control. pIRE1α, phosphorylated IRE1α. (**B**) Expression of SCD1 mRNA was measured by quantitative real-time PCR. The expression level of gene was normalized to expression of GAPDH gene and is represented as fold change over control siRNA transfected cells.

The data represents the mean ± SEM (n=3). *$p<0.05$, ***$p<0.001$.

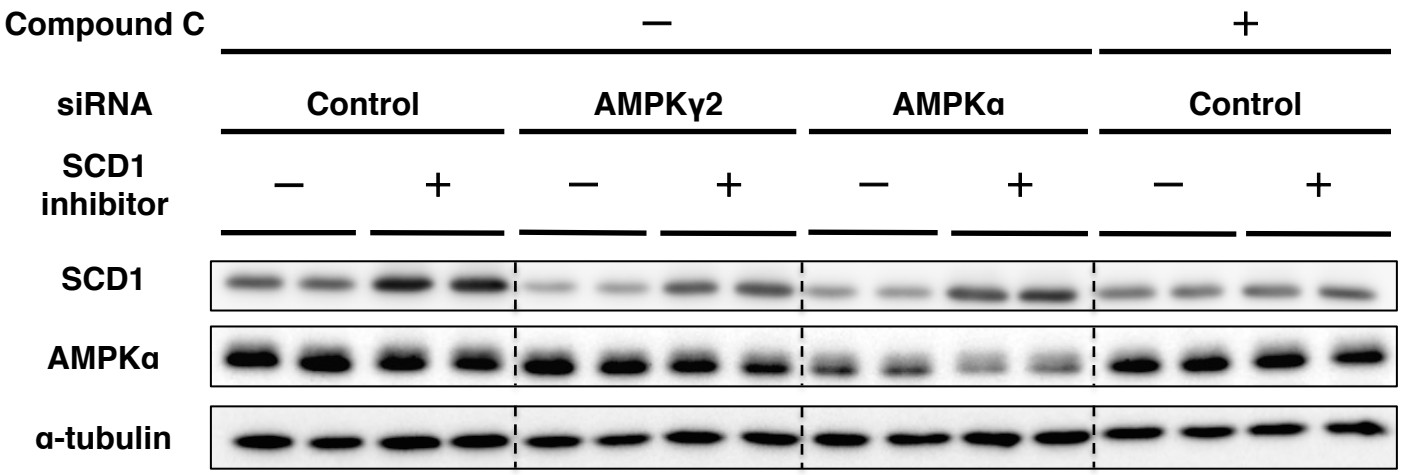

Figure 26. SCD1 expression is elevated by SCD1 inhibitor treatment in an AMPK-dependent manner

HeLa cells were transfected with the indicated siRNAs. At 72 h after transfection, cells were treated with SCD1 inhibitor (5 μM) and Compound C (10 μM) for 24 h and then harvested. Whole cell lysates were subjected to immunoblot analysis using indicated antibodies. α-tubulin was used as a loading control.

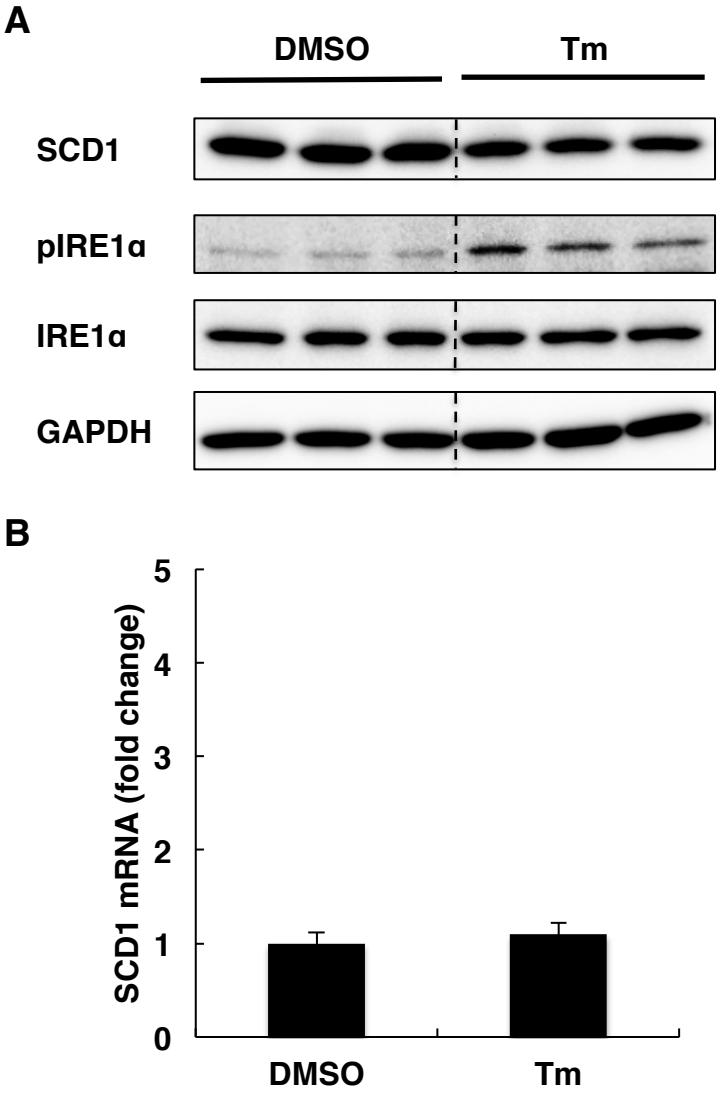

Figure 27. Tunicamycin treatment does not change SCD1 expression

HeLa cells were treated with tunicamycin (2.5μg/ml) for 4h and then harvested. (**A**) Whole cell lysates were subjected to immunoblot analysis using indicated antibodies. GAPDH was used as a loading control. pIRE1α, phosphorylated IRE1α. (**B**) Expression of SCD1 mRNA was measured by quantitative real-time PCR. The expression level of gene was normalized to expression of GAPDH gene and is represented as fold change over control cells.

The data represents the mean ± SEM (n=3).

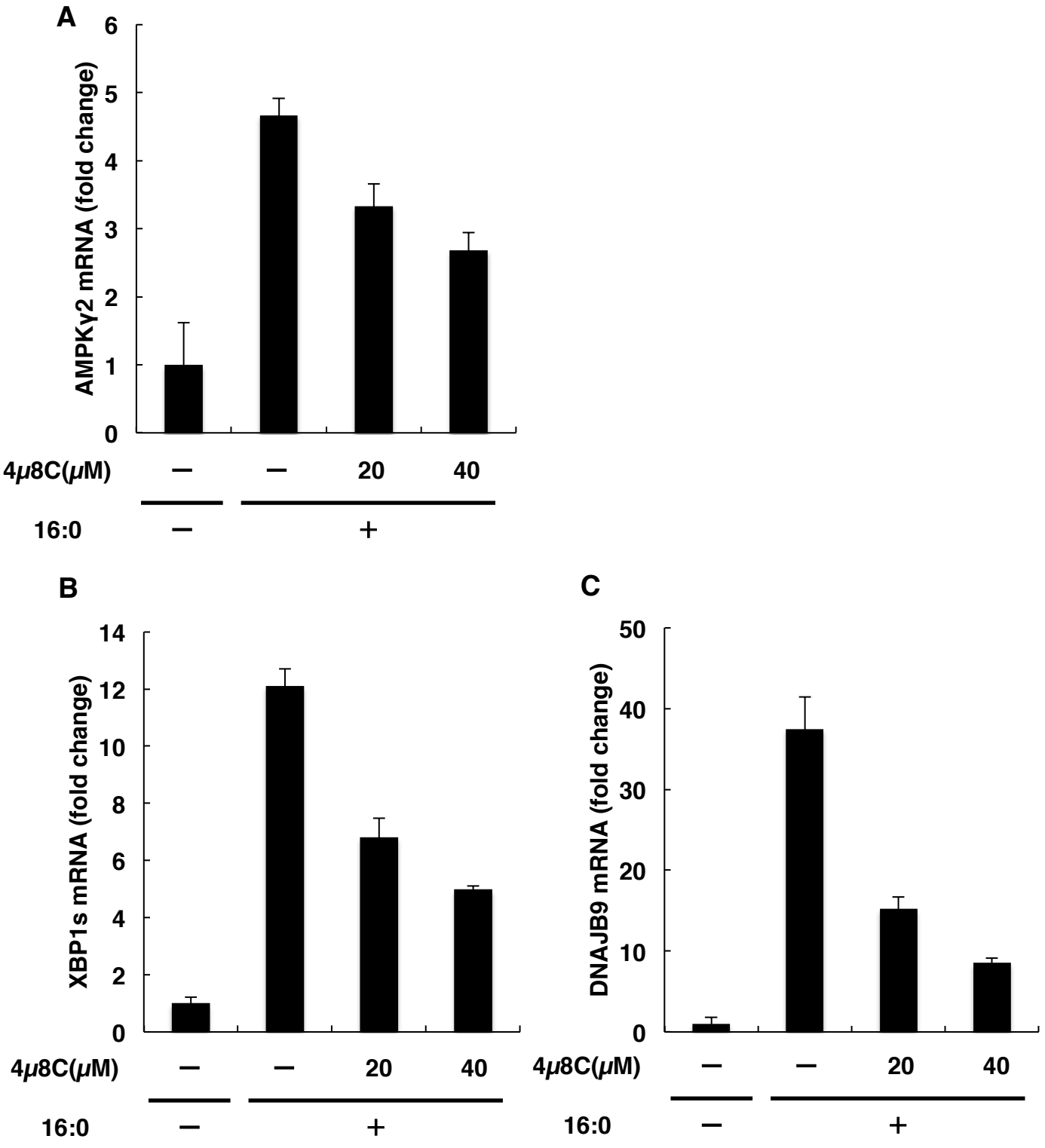

Figure 28. The effect of IRE1 inhibitor on AMPKγ2 expression

(**A-C**) HeLa cells were treated with 16:0 (100 μM) and 4μ8C for 12 h and then harvested. Expression of AMPKγ2 (**A**), XBP1s (**B**) and DNAJB9 (**C**) mRNA was measured by quantitative real-time PCR. The expression level of gene was normalized to expression of GAPDH gene and is represented as fold change over untreated cells.

The data represents the mean ± SEM (n=3).

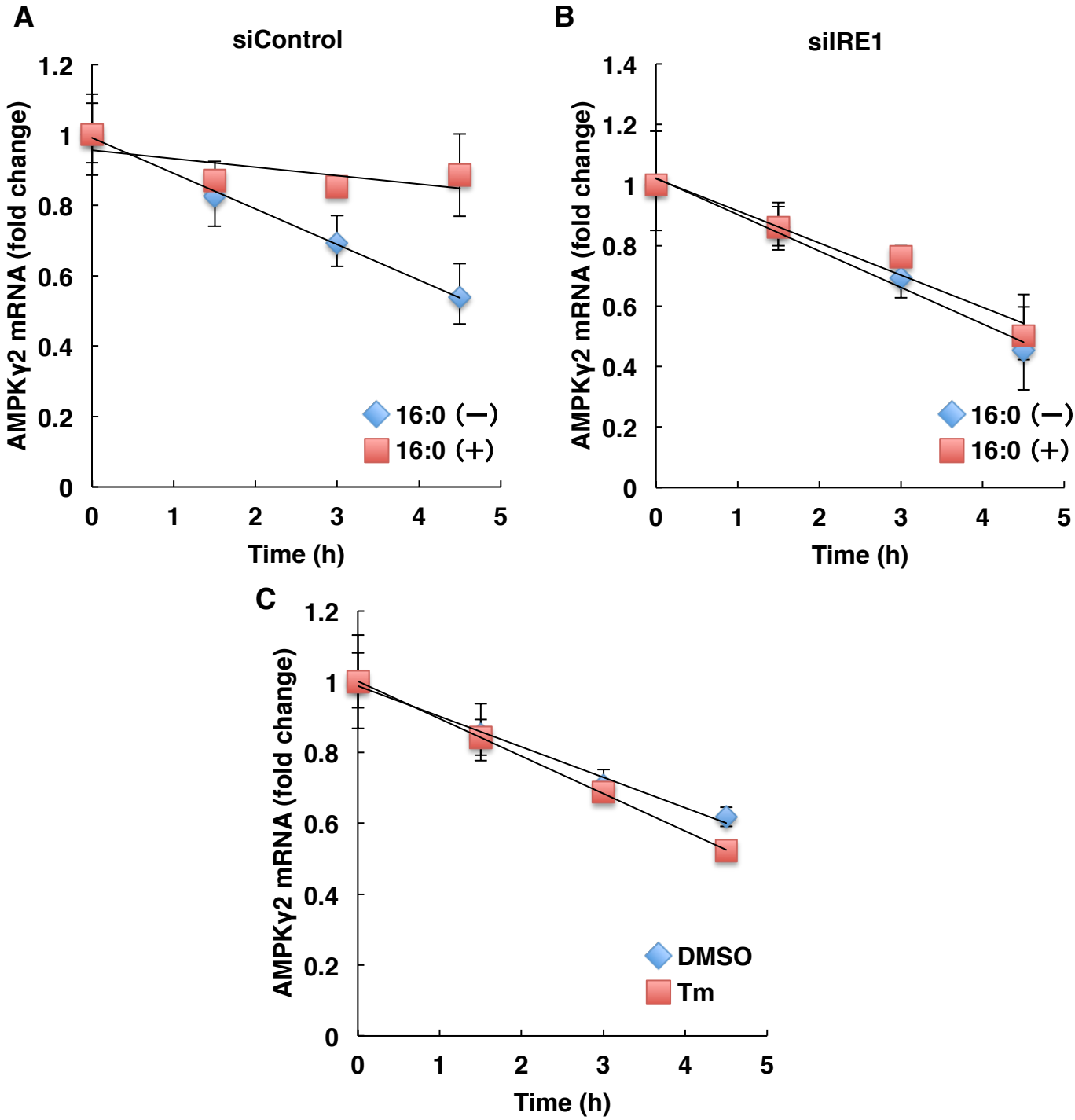

Figure 29. The stability of AMPKγ2 mRNA in HeLa cells

(**A, B**) HeLa cells were transfected with the indicated siRNAs. At 72 h after transfection, cells were pretreated with 16:0 (100 μM) for 7.5 h, then treated with Actinomycin D (5 μg/mL) and 16:0 (100 μM) for indicated duration.

(**C**) HeLa cells were pretreated with tunicamycin (2.5 μg/mL) for 2 h, then treated with Actinomycin D (5 μg/mL) and tunicamycin (2.5 μg/mL) for indicated duration.

Expression of AMPKγ2 mRNA was measured by quantitative real-time PCR. The expression level of gene was normalized to expression of GAPDH gene and is represented as fold change over time zero point. The data represents the mean ± SEM (n=3).

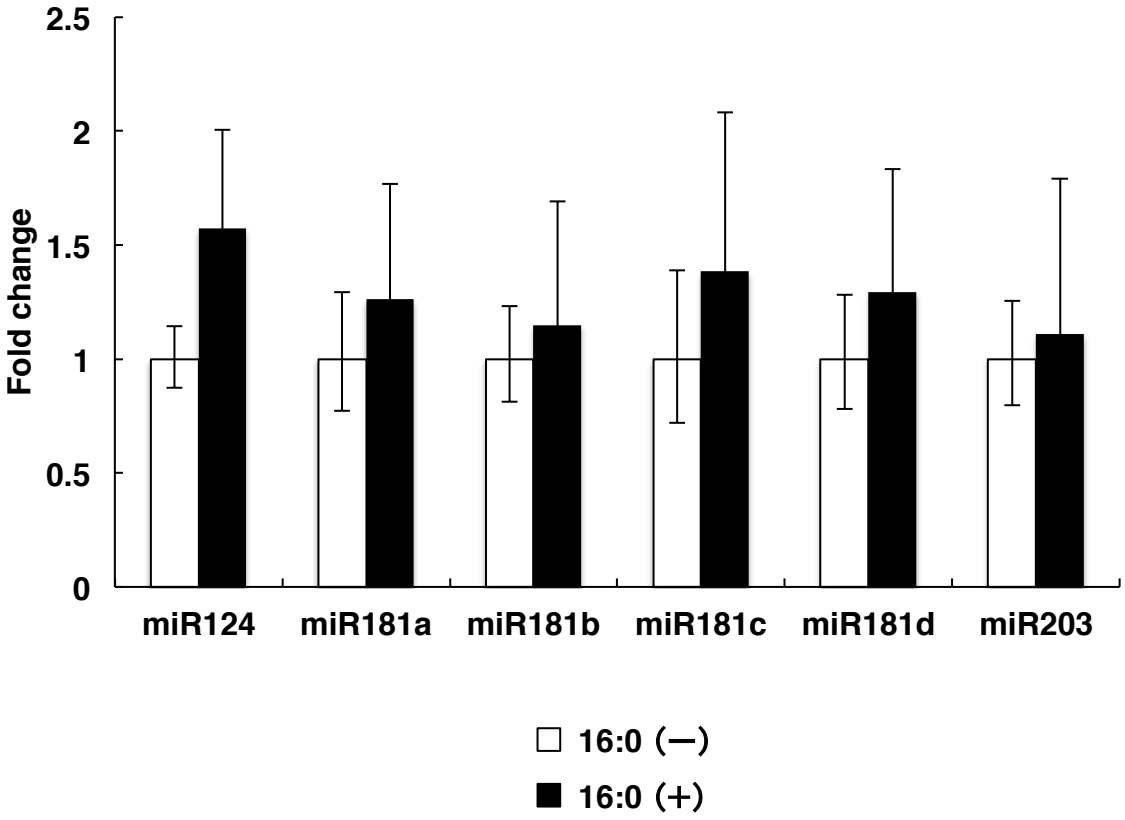

Figure 30. The amount of miRNAs, predicted to target AMPKγ2 mRNA, in HeLa cells
HeLa cells were treated with 16:0 (100 μM) for 12 h and then harvested. Expression of indicated miRNA was measured by quantitative real-time PCR. The expression level of gene was normalized to expression of U6 snoRNA and is represented as fold change over control cells. The data represents the mean ± SEM (n=3).

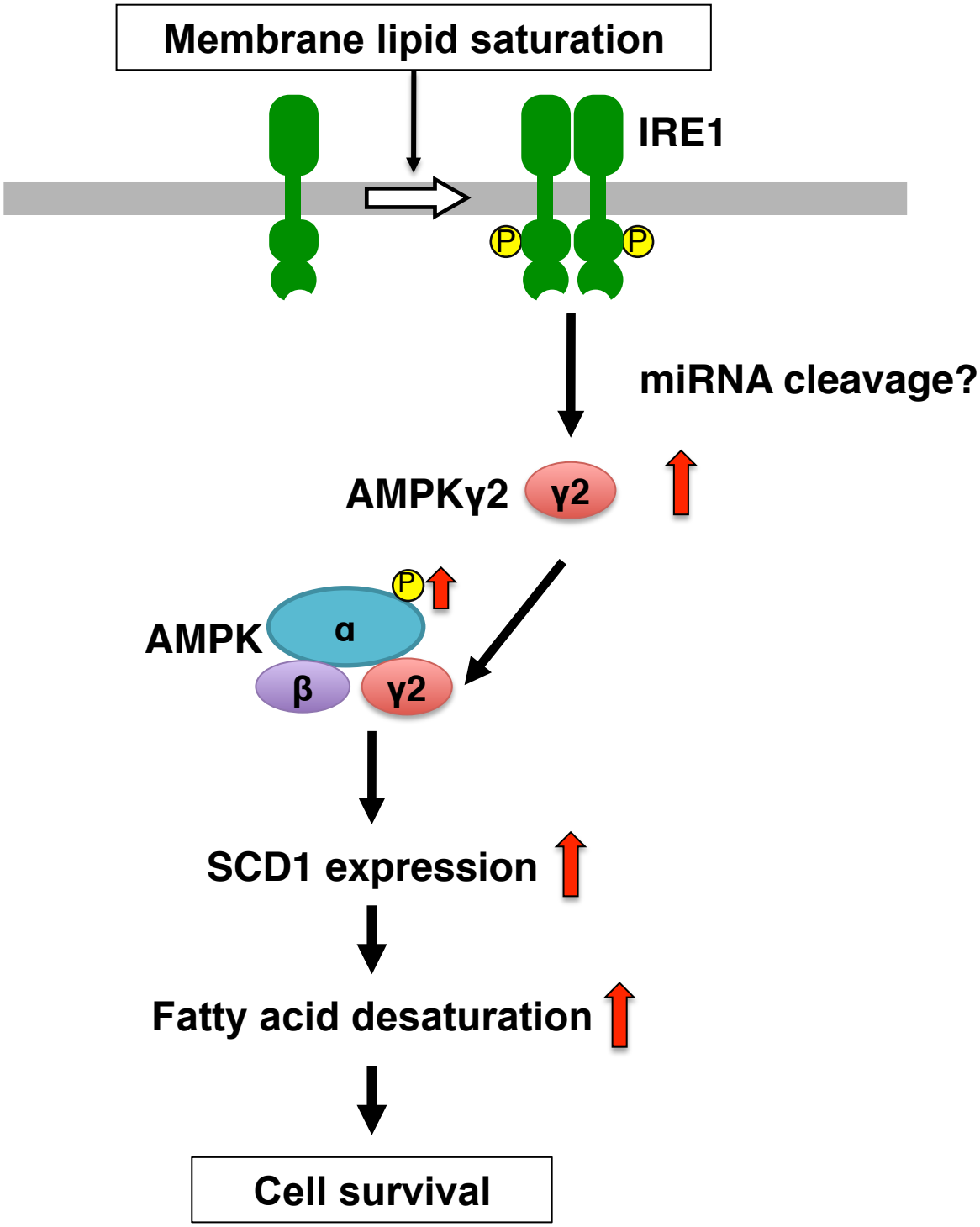

Figure 31. Summary

In membrane lipid saturation but not unfolded protein accumulation, AMPKγ2 is up-regulated by a UPR sensor IRE1. Increasing AMPKγ2 expression is independent of XBP1. AMPKγ2 up-regulation enhances phosphorylation of AMPKα, which causes SCD1 up-regulation and facilitates saturated fatty acid desaturation. This response is required for membrane lipid homeostasis and cell survival .

Material and Methods

Reagents

All chemicals were purchased from Wako Pure Chemicals (Osaka, Japan) unless otherwise stated. Palmitic acid (16:0) was purchased from Cayman Chemicals (Ann Arbor, MI). [1-^{14}C]-labeled 16:0 was obtained from American Radiolabeled Chemicals (St.Louis, MO). Dulbecco's modified Eagle's medium was obtained from Life Technologies (Gaithersburg, MD). SCD1 inhibitor (CAY10566) was purchased from Santa Cruz Biotechnology (Santa Cruz, CA). Tunicamycin and anti-α-tubulin were obtained from Sigma. Anti-SCD1 was purchased from Advanced Targeting Systems (San Diego, CA). Anti-IRE1α, anti-AMPKα, anti-phospho-AMPKα, anti-Caspase3, anti-cleaved Caspase3 were obtained from Cell signaling technology (Beverly, MA). Anti-GAPDH and 4μ8C (IRE1 inhibitor) were obtained from Calbiochem (San Diego, CA). Anti-phospho-IRE1α and Compound C were purchased from Abcam (Cambridge, MA). A control small interfering RNA (siRNA) and siRNAs directed against IRE1, PERK, AMPKα1, AMPKα2, and AMPKγ2 were obtained from Nippon EGT (Toyama, Japan). An siRNA directed against XBP1 was purchased from Life technologies.

Cell culture and transfection

HeLa cells were maintained in DMEM supplemented with 10% fetal bovine serum and 100 units/mL penicillin, 100 mg/mL streptomycin, and 2 mM L-glutamine. siRNAs were transfected into HeLa cells with Lipofectamine^{TM} RNAiMAX (Life technologies) according to the manufacture's protocol. Plasmids were transfected into HeLa cells with

Lipofectamine™ 2000 (Life technologies) according to the manufacture's protocol. HeLa cells stably expressing XBP1s were generated as follows: HEK293T cells were transiently transfected using Lipofectamine™ 2000 with pMRX-puro-XBP1s together with pCG-VSV-G and pCG-gag-pol to render retroviruses infectious to human cells. HeLa cells were infected with the retrovirus, and selected using puromycin. For palmitic acid treatment the cells were incubated in the identical medium with fatty acid at indicated concentration or solvent (ethanol) for indicated time periods before analysis.

Total RNA isolation and Quantitative real-time PCR

Total RNA was extracted from cells using Isogen II (Nippon- gene, Toyama, Japan) and reverse-transcribed using the High- Capacity cDNA Reverse Transcription kit (Life technologies). Quantitative real-time PCR was carried out using SYBR Green PCR Master Mix (Roche Diagnostics, Basel, Switzer- land) and LightCycler 480 (Roche Diagnostics). The sequences of the oligonucleotides were as follows. DNAJB9 forward (ATC AGA GCG CCA AAT CAA GAA GG) and reverse (TTC AGC ATC CGG GCT CTT ATT TTT G), XBP1s forward (CCG CAG CAG GTG CAG G) and reverse (GAG TCA ATA CCG CCA GAA TCC A), AMPKγ2 forward (GAG GAC GAA GCA GTA GAA GAC TC) and reverse (GGC TAC CAA AGC AAA GAA GGC), FBXO16 forward (GCC TAA GAC ACC CCC AAA GG) and reverse (TGC TTT CTC CCC TGA GTT ATT CTT C), PPAPDC1B forward (CCA CCA AGC CGA TGT TTG TTA TTG) and reverse (TGC TGT CTC TTG TGT CTG CC), TMEM39A forward (AGG

CTT GAG AAA CAG GAA TGG TAG) and reverse (CTC CCA TCC ACA GGC AAG TC), AMIGO3 forward (ACA CCC CAG GAC AGA AAG AGG) and reverse (TTT CAG GAG GTT GGG TGT TGG), FKBP14 forward (GGC TCC TTA TTT CAC TCC ACT CAC) and reverse (AAG CCC TGG TCC CAA CCT TT), SEC24D forward (GCT CAC TGG AGG AAC CCT TTA C) and reverse (TGG CTC TGA AAC CTG TGC TG), RWDD2A forward (CAG ATT GAA GAG CCC AAG GTG A) and reverse (AGA AGT GAG ACC TTT GTT GAG AAG T), PGM3 forward (AAG ACA AGC AGT TAC ACC CCC) and reverse (GCA CTT TCT TGT GAG TCT GCT TC), PRSS16 forward (TTC CCG AGC AGA GAC AGT GG) and reverse (ACA GGT GAC ATA GAA GCC GAA C) and GAPDH forward (GCC AAG GTC ATC CAT GAC AAC T) and reverse (GAG GGG CCA TCC ACA GTC TT). Target gene expression was normalized on the basis of GAPDH content. Relative quantities of mature miRNAs were determined using Applied Biosystems TaqMan® microRNA Assays.

Immunoblotting

HeLa cells were lysed in lysis buffer (62.5 mM Tris-HCl, pH 6.8, 2% w/v SDS, 10% glycerol, 137 mM NaCl, 2 mM EDTA) containing the Complete EDTA-free protease inhibitor cocktail (Roche) and Phos-Stop (Roche) for 15min on ice, followd by sonication. After centrifugation, the supernatants were used as total protein extracts. The protein concentrations of the samples were determined by the bicinchoninic acid (BCA) assay (Pierce). Each total protein extract (20 μg/lane) was subjected to SDS-PAGE and immunoblotting. The following dilutions of primary antibodies were used

for immunoblotting: anti-phospho-IRE1α (1:1000), anti-IRE1α (1:1000), anti-phospho-AMPKα (1:1000), anti-AMPKα (1:1000), anti-Caspase3 (1:1000), anti-cleaved Caspase3 (1:1000), anti-SCD1 (1:1000), anti-GAPDH (1:2000) and anti-α-tubulin (1:5000).

Lipid analysis

Lipids were extracted from cells by the method of Bligh and Dyer (Bligh and Dyer, 1959). Then lipids were transmethylated with 2.5% H_2SO_4 in methanol. The resulting fatty acid methyl esters were then extracted with hexane and subjected to gas chromatography-mass spectrometry (GC-MS) analysis. GC-MS analysis was performed by using an Agilent 7890A-5975C GC-MS network system (Agilent Technologies, Wilmington, DE) equipped with a DB-23 capillary column (60 m × 250 μm × 0.15 μm; Agilent Technologies). The oven temperature program was as follows: the initial temperature was 50°C for 1 min, then raised to 175 °C at 25 °C/min, to 235 °C at 5 °C/min and held for 5 min. The injector and detector temperatures were both set at 250 °C.

***In vivo* incorporation of exogenous fatty acids into HeLa cells**

HeLa cells were plated in six-well dishes and incubated for 24hours. siRNAs were then transfected into cells. After incubation for 72 hours, the cells were wash and 100μM palmitic acid including [^{14}C] palmitic acid (0.1μCi/well) was added to the medium as an albumin complex. After incubation for 12 hours, cellular lipids were extracted by the

method of Bligh and Dyer (Bligh and Dyer, 1959) and transmethylated with 2.5% H_2SO_4 in methanol. The resulting fatty acid methyl esters were then separated by 40% $AgNO_3$-coated TLC in hexane:diethyl ether:acetic acid (94:4:2, v/v). Desaturated [^{14}C] palmitic acid was expressed as the percentage of radioactivity incorporated into total fatty acid methyl esters.

Microarray analysis

Isolated RNA was further purified with RNeasy Mini Kit (Qiagen, Valencia, CA). Then RNA expression array were performed using the Agilent Sure Print G3 Human GE 8x60K v2 Microarray.

Plasmid construction

AMPKγ2 and XBP1s genes were amplified by polymerase chain reaction (PCR) with cDNA derived from HeLa cells using the following primers:

5'-GCG AAT TCA TGG GAA GCG CGG TTA TGG ACA CC-3' and

5'-GCC TCG AGT CTC CGT TTC TGT CTC CTT TTG TTT GG-3' (AMPKγ2);

5'-CGG GAT CCA TGG TGG TGG TGG CAG CCG CGC C-3' and

5'- GGT TTA GCG GCC GCT TAG ACA CTA ATC AGC TGG GG-3' (XBP1s).

AMPKγ2 cDNA was introduced into pcDNA3 with Myc-tag (C-terminal) and pCAGGS with FLAG-tag (C-terminal). XBP1s cDNA was introduced into pMRX-Puro.

References

Ariyama H. et al. (2010). Decrease in membrane phospholipid unsaturation induces unfolded protein response. *J Biol Chem* **285**, 22027–22035.

Bandyopadhyay G.K. et al. (2006). Increased malonyl-CoA levels in muscle from obese and type 2 diabetic subjects lead to decreased fatty acid oxidation and increased lipogenesis; thiazolidinedione treatment reverses these defects. *Diabetes* **55**, 2277–2285.

Bligh E.G. and Dyer W.J. (1959). A rapid method of total lipid extraction and purification. *Can J Biochem Physiol* **37**, 911-917.

Bommiasamy S.H. et al. (2009). ATF6 α induces XBP1-independent expansion of the endoplasmic reticulum. *J Cell Sci* **122**, 1626–1636.

Calfon M. et al. (2002). IRE1 couples endoplasmic reticulum load to secretory capacity by processing the XBP-1 mRNA. *Nature* **415**, 92-96.

Canto C. et al. (2010). Interdependence of AMPK and SIRT1 for metabolic adaptation to fasting and exercise in skeletal muscle. *Cell Metab* **11**, 213–219.

Kato H. et al. (2006). Ubiquitin-proteasome-dependent degradation of mammalian ER stearoyl-CoA desaturase. *J Cell Sci* **119**, 2342-2353.

Cazanave S.C. et al. (2009). JNK1-dependent PUMA expression contributes to hepatocyte lipoapoptosis. *J Biol Chem* **284,** 26591–26602.

Cheung P.C.F et al. (2000). Characterization of AMP-activated protein kinase γ subunit isoforms and their role in AMP binding. *Biochem J* **346**, 659-669.

Cox J.S. and Walter P. (1996). A novel mechanism for regulating activity of a transcription factor that controls the unfolded protein response. *Cell* **87**, 391-404.

Cross B.C. et al. (2012). The molecular basis for selective inhibition of unconventional mRNA splicing by an IRE1-binding small molecule. *Proc Natl Acad Sci USA* **109**, E869–E878.

Folmes K.D. et al. (2009). Distinct early signaling events resulting from the expression of the PRKAG2 R302Q mutant of AMPK contribute to increased myocardial glycogen. *Circ Cardiovasc Genet* **2**, 457–466.

Gregor M.F. et al. (2009). Endoplasmic reticulum stress is reduced in tissues of obese subjects after weight loss. *Diabetes* **58**, 693–700.

Hardie D.G. et al. (2012). AMPK: a nutrient and energy sensor that maintains energy homeostasis. *Nature Rev Mol Cell Biol* **13**, 251–262.

Hawley S.A. et al. (2005). Calmodulin-dependent protein kinase kinase beta is an alternative upstream kinase for AMP-activated protein kinase. *Cell Metab* **2**, 9–19.

Holub B.J. and Kuksis A. (1978). Metabolism of molecular species of diacylglycerophospholipids. *Adv Lipid Res* **16**, 1-125.

Holzer R.G. et al. (2011). Saturated fatty acids induce c-Src clustering within membrane subdomains, leading to JNK activation. *Cell* **147**, 173–184.

Inaba M. et al. (2003). Gene-engineered rigidification of membrane lipids enhances the cold inducibility of gene expression in synechocystis. *J Biol Chem* **278**, 12191-12198.

Jager S. et al. (2007). AMP-activated protein kinase (AMPK) action in skeletal muscle via direct phosphorylation of PGC-1alpha. *Proc Natl Acad Sci USA* **104**, 12017–12022.

Kitai Y. et al. (2013). Membrane lipid saturation activates IRE1alpha without inducing clustering. *Genes Cells* **18**, 798–809.

Lands W.E. and Crawford C.G. (1976). Enzymes of membrane phospholipid metabolism in animals. *The Enzymes of Biological Membranes Vol. II*, 3–85.

Lerner A.G. et al. (2012). IRE1α induces thioredoxin-interacting protein to activate the NLRP3 inflammasome and promote programmed cell death under irremediable ER stress. *Cell Metab* **16**, 250–264.

Lin J. et al. (2005). Metabolic control through the PGC-1 family of transcription coactivators. *Cell Metab* **1**, 361–370.

Liu G. et al. (2007). Discovery of potent, selective, orally bioavailable stearoyl-CoA desaturase 1 inhibitors. *J Med Chem* **50**, 3086-3100.

MacDonald J.I. and Sprecher H. (1991). Phospholipid fatty acid remodeling in mammalian cells. *Biochim Biophys Acta* **1084**, 105-121.

Malhi H. et al. (2006). Free fatty acids induce JNK-dependent hepatocyte lipoapoptosis. *J Biol Chem* **281**, 12093–12101.

Maurel M. et al. (2014). Getting RIDD of RNA: IRE1 in cell fate regulation. *Trends Biochem Sci* **39**, 245–254.

Mauvoisin D. and Mounier C. (2011). Hormonal and nutritional regulation of SCD1 gene expression. *Biochimie* **93**, 78–86.

Marciniak S.J. et al. (2004). CHOP induces death by promoting protein synthesis and oxidation in the stressed endoplasmic reticulum. *Genes Dev* **18**, 3066-3077.

McCullough K.D. et al. (2001). Gadd153 sensitizes cells to endoplasmic reticulum stress by down-regulating Bcl2 and perturbing the cellular redox state. *Mol Cell Biol* **21**, 1249-1259.

Meares G.P. et al. (2011). IRE1-dependent activation of AMPK in response to nitric oxide. *Mol Cell Biol* **31**, 4286-4297.

Mihaylova M.M. and Shaw R.J. (2011). The AMPK signalling pathway coordinates cell growth, autophagy and metabolism. *Nature Cell Biol* **13**, 1016–1023.

Moffat C. and Harper M.E. (2010). Metabolic functions of AMPK: aspects of structure and of natural mutations in the regulatory gamma subunits. *IUBMB Life* **62**, 739–745.

Momcilovic M. et al. (2006). TAK1 activates Snf1 protein kinase in yeast and phosphorylates AMP-activated protein kinase in vitro. *J Biol Chem* **281**, 25336–25343.

Nathan D.M. et al. (2009). Medical management of hyperglycaemia in type 2 diabetes mellitus: a consensus algorithm for the initiation and adjustment of therapy: a consensus statement from the American Diabetes Association and the European Association for the Study of Diabetes. *Diabetologia* **52**, 17–30.

Nishitoh H. et al. (2002). ASK1 is essential for endoplasmic reticulum stress-induced neuronal cell death triggered by expanded polyglutamine repeats. *Genes Dev* **16**, 1345–1355.

Okoshi R. et al. (2008). Activation of AMP-activated protein kinase induces p53-dependent apoptotic cell death in response to energetic stress. *J Biol Chem* **283**, 3979–3987.

Ozcan U. et al. (2004). Endoplasmic reticulum stress links obesity, insulin action, and type 2 diabetes. *Science* **306**, 457–461.

Ozcan U. et al. (2006). Chemical chaperones reduce ER stress and restore glucose homeostasis in a mouse model of type 2 diabetes. *Science* **313**, 1137–1140.

Puri P. et al. (2008). Activation and dysregulation of the unfolded protein response in nonalcoholic fatty liver disease. *Gastroenterology* **134**, 568–576.

Rena G. et al. (2013). Molecular mechanism of action of metformin: old or new insights? *Diabetologia* **56**, 1898–1906.

Ron D. and Walter P. (2007). Signal integration in the endoplasmic reticulum unfolded protein response. *Nature Rev Mol Cell Biol* **8**, 519–529.

Shi H. et al. (2006). TLR4 links innate immunity and fatty acid-induced insulin resistance. *J Clin Invest* **116**, 3015–3025.

Spector A.A. and Yorek M.A. (1985). Membrane lipid composition and cellular function. *J Lipid Res* **26**, 1015-1035.

Sriburi R. et al. (2004). XBP1: a link between the unfolded protein response, lipid biosynthesis, and biogenesis of the endoplasmic reticulum. *J Cell Biol* **167**, 35–41.

Sriburi R. et al. (2007). Coordinate regulation of phospholipid biosynthesis and secretory pathway gene expression in XBP-1(S)-induced endoplasmic reticulum biogenesis. *J Biol Chem* **282**, 7024–7034.

Upton J.P. et al. (2012) IRE1α cleaves select microRNAs during ER stress to derepress translation of proapoptotic caspase-2. *Science* **338**, 818–822.

Urano F. et al. (2000). Coupling of stress in the ER to activation of JNK protein kinases by transmembrane protein kinase IRE1. *Science* **287**, 664–666.

Vigh L. et al. (1993). The primary signal in the biological perception of temperature: Pd-catalyzed hydrogenation of membrane lipids stimulated the expression of the desA gene in Synechocystis PCC6803. *Proc Natl Acad Sci U S A* **90**, 9090-9094.

Walter P. and Ron D. (2011). The unfolded protein response: from stress pathway to homeostatic regulation. *Science* **334**, 1081–1086.

Wilson R. and Sargent J.R. (2001). Chain separation of monounsaturated fatty acid methyl esters by argentation thin-layer chromatography. *J Chromatogr A* **905**, 251–257.

Woods A. et al. (2003). LKB1 is the upstream kinase in the AMP-activated protein kinase cascade. *Curr Biol* **13**, 2004–2008.

Xiao B. et al. (2013). Structural basis of AMPK regulation by small molecule activators. *Nat Commun* **4**, 3017.

Xu X.J. et al. (2012). Insulin sensitive and resistant obesity in humans: AMPK activity, oxidative stress, and depot-specific changes in gene expression in adipose tissue. *J Lipid Res* **53**, 792–801.

Zhou G. et al. (2011). Role of AMP-activated protein kinase in mechanism of metformin action. *J Clin Invest* **108**, 1167–1174.

Acknowledgements

I am grateful to Professor Dr. H. Arai and Dr. N. Kono for their supervisions of over my 6 years of research. Also, I am grateful to Dr. T. Taguchi, Dr. R. Imae, Dr. M. Arita (RIKEN) and Dr. T Inoue (National Institute of Health Science) for all the support.

I gratefully acknowledge technical assistance from Mrs. Fukuda, Mrs. Akimura and Mrs. Takada. I also thank to all the member of Arai's lab for helpful discussions and their encouragement. Finally, my special thanks go to my parents.